ϕ-meson photoproduction on hydrogen in the neutral decay mode

H. Seraydaryan,[1] M. J. Amaryan,[1,*] G. Gavalian,[1] H. Baghdasaryan,[2] L. Weinstein,[1] K. P. Adhikari,[1] D. Adikaram,[1] M. Aghasyan,[3] M. D. Anderson,[4] S. Anefalos Pereira,[3] H. Avakian,[5] J. Ball,[6] N. A. Baltzell,[7,8] M. Battaglieri,[9] V. Batourine,[5,10] I. Bedlinskiy,[11] R. P. Bennett,[1] A. S. Biselli,[12] J. Bono,[13] S. Boiarinov,[5] W. J. Briscoe,[14] W. K. Brooks,[15,5] S. Bültmann,[1] V. D. Burkert,[5] D. S. Carman,[5] A. Celentano,[9] S. Chandavar,[16] P. Collins,[17] M. Contalbrigo,[18] O. Cortes,[19] V. Crede,[20] A. D'Angelo,[21,22] N. Dashyan,[23] R. De Vita,[9] E. De Sanctis,[3] A. Deur,[5] C. Djalali,[8] D. Doughty,[24,5] M. Dugger,[25] R. Dupre,[26] L. El Fassi,[7] P. Eugenio,[20] G. Fedotov,[8,27] S. Fegan,[9] R. Fersch,[28,†] J. A. Fleming,[29] N. Gevorgyan,[23] K. L. Giovanetti,[30] F. X. Girod,[5,6] J. T. Goetz,[16] W. Gohn,[31] E. Golovatch,[27] R. W. Gothe,[8] K. A. Griffioen,[28] M. Guidal,[26] N. Guler,[1,‡] L. Guo,[13,5] K. Hafidi,[7] H. Hakobyan,[15,23] C. Hanretty,[32,20] N. Harrison,[31] D. Heddle,[24,5] K. Hicks,[16] D. Ho,[33] M. Holtrop,[34] C. E. Hyde,[1] Y. Ilieva,[8,14] D. G. Ireland,[4] B. S. Ishkhanov,[27] E. L. Isupov,[27] H. S. Jo,[26] K. Joo,[31] D. Keller,[32] M. Khandaker,[35] A. Kim,[10] W. Kim,[10] F. J. Klein,[17] S. Koirala,[1] A. Kubarovsky,[31,27] V. Kubarovsky,[5,36] S. E. Kuhn,[1] S. V. Kuleshov,[15,11] S. Lewis,[4] K. Livingston,[4] H. Y. Lu,[33,8] I. J. D. MacGregor,[4] D. Martinez,[19] M. Mayer,[1] B. McKinnon,[4] T. Mineeva,[31] M. Mirazita,[3] V. Mokeev,[5,27,§] R. A. Montgomery,[4] H. Moutarde,[6] E. Munevar,[5,14] C. Munoz Camacho,[26] P. Nadel-Turonski,[5] R. Nasseripour,[30,8] S. Niccolai,[26] I. Niculescu,[30] M. Osipenko,[9] A. I. Ostrovidov,[20] L. L. Pappalardo,[18] R. Paremuzyan,[23,‖] K. Park,[5,10] S. Park,[20] E. Pasyuk,[5,25] E. Phelps,[8] J. J. Phillips,[4] S. Pisano,[3] O. Pogorelko,[11] S. Pozdniakov,[11] J. W. Price,[37] D. Protopopescu,[4] A. J. R. Puckett,[5] D. Rimal,[13] M. Ripani,[9] B. G. Ritchie,[25] A. Rizzo,[22] G. Rosner,[4] P. Rossi,[3,5] F. Sabatié,[6] M. S. Saini,[20] C. Salgado,[35] D. Schott,[14] R. A. Schumacher,[33] E. Seder,[31] Y. G. Sharabian,[5] G. D. Smith,[4] D. I. Sober,[17] D. Sokhan,[4,29] S. Stepanyan,[5] P. Stoler,[36] I. I. Strakovsky,[14] S. Strauch,[8,14] W. Tang,[16] C. E. Taylor,[19] Ye Tian,[8] S. Tkachenko,[32,1] M. Ungaro,[5] M. F. Vineyard,[38] H. Voskanyan,[23] E. Voutier,[39] N. K. Walford,[17] D. P. Watts,[29] L. B. Weinstein,[1] M. H. Wood,[40,8] N. Zachariou,[8] L. Zana,[34] J. Zhang,[5] and Z. W. Zhao[32]

(CLAS Collaboration)

[1]*Old Dominion University, Norfolk, Virginia 23529, USA*
[2]*University of Virginia, Charlottesville, Virginia 22904, USA*
[3]*INFN, Laboratori Nazionali di Frascati, 00044 Frascati, Italy*
[4]*University of Glasgow, Glasgow G12 8QQ, United Kingdom*
[5]*Thomas Jefferson National Accelerator Facility, Newport News, Virginia 23606, USA*
[6]*CEA, Centre de Saclay, Irfu/Service de Physique Nucléaire, 91191 Gif-sur-Yvette, France*
[7]*Argonne National Laboratory, Argonne, Illinois 60439, USA*
[8]*University of South Carolina, Columbia, South Carolina 29208, USA*
[9]*INFN, Sezione di Genova, 16146 Genova, Italy*
[10]*Kyungpook National University, Daegu 702-701, Republic of Korea*
[11]*Institute of Theoretical and Experimental Physics, Moscow 117259, Russia*
[12]*Fairfield University, Fairfield, Connecticut 06824, USA*
[13]*Florida International University, Miami, Florida 33199, USA*
[14]*The George Washington University, Washington, DC 20052, USA*
[15]*Universidad Técnica Federico Santa María, Casilla 110-V Valparaíso, Chile*
[16]*Ohio University, Athens, Ohio 45701, USA*
[17]*Catholic University of America, Washington, DC 20064, USA*
[18]*INFN, Sezione di Ferrara, 44100 Ferrara, Italy*
[19]*Idaho State University, Pocatello, Idaho 83209, USA*
[20]*Florida State University, Tallahassee, Florida 32306, USA*
[21]*INFN, Sezione di Roma Tor Vergata, 00133 Rome, Italy*
[22]*Universita' di Roma Tor Vergata, 00133 Rome, Italy*
[23]*Yerevan Physics Institute, 375036 Yerevan, Armenia*
[24]*Christopher Newport University, Newport News, Virginia 23606, USA*
[25]*Arizona State University, Tempe, Arizona 85287-1504, USA*
[26]*Institut de Physique Nucléaire ORSAY, Orsay, France*
[27]*Skobeltsyn Nuclear Physics Institute, 119899 Moscow, Russia*
[28]*College of William and Mary, Williamsburg, Virginia 23187-8795, USA*
[29]*University of Edinburgh, Edinburgh EH9 3JZ, United Kingdom*
[30]*James Madison University, Harrisonburg, Virginia 22807, USA*
[31]*University of Connecticut, Storrs, Connecticut 06269, USA*
[32]*University of Virginia, Charlottesville, Virginia 22901, USA*
[33]*Carnegie Mellon University, Pittsburgh, Pennsylvania 15213, USA*
[34]*University of New Hampshire, Durham, New Hampshire 03824-3568, USA*
[35]*Norfolk State University, Norfolk, Virginia 23504, USA*
[36]*Rensselaer Polytechnic Institute, Troy, New York 12180-3590, USA*

[37]*California State University, Dominguez Hills, Carson, California 90747, USA*
[38]*Union College, Schenectady, New York 12308, USA*
[39]*LPSC, Universite Joseph Fourier, CNRS/IN2P3, INPG, Grenoble, France*
[40]*Canisius College, Buffalo, New York 14208, USA*
(Received 7 August 2013; revised manuscript received 17 March 2014; published 22 May 2014)

We report the first measurement of the photoproduction cross section of the ϕ meson in its neutral decay mode in the reaction $\gamma p \to p\phi(K_S K_L)$. The experiment was performed with a tagged photon beam of energy $1.6 \leqslant E_\gamma \leqslant 3.6$ GeV incident on a liquid hydrogen target of the CLAS spectrometer at the Thomas Jefferson National Accelerator Facility. The $p\phi$ final state is identified via reconstruction of K_S in the invariant mass of two oppositely charged pions and by requiring the missing particle in the reaction $\gamma p \to pK_S X$ to be K_L. The presented results significantly enlarge the existing data on ϕ photoproduction. These data, combined with the data from the charged decay mode, will help to constrain different mechanisms of ϕ photoproduction.

DOI: 10.1103/PhysRevC.89.055206 PACS number(s): 12.38.Aw, 13.60.Rj, 14.20.−c, 25.20.Lj

I. INTRODUCTION

Strangeness production at low photon energy starting from threshold is very interesting for different reasons. On one hand, it is an energy domain well above the region controlled by low-energy theorems [1]; on the other hand, it is far below the region of perturbative QCD [2–4]. In this energy range various baryon resonances and coupled-channel effects may play an important role in strangeness photoproduction [5–9]. Moreover, it is important to conduct strangeness production experiments to establish the quantum numbers of the known states, as well as to search for so-called missing baryon resonances [10–14].

Because the ϕ meson is a particle with hidden strangeness it can be produced without an associated hyperon. The Okubo-Iizuka-Zweig (OZI) rule states that although the $\phi \to \pi^+\pi^-\pi^0$ meson decay has more phase space available, compared to $\phi \to K\bar{K}$, it is suppressed owing to the fact that $s\bar{s}$ could decay to 3π only via disconnected quark graphs, which involves gluons. Similarly, owing to the suppressed strange quark content of the nucleon, ϕ-meson photoproduction on a nucleon should proceed via disconnected quark graphs and therefore is sensitive to processes involving gluons [15]. The same argument is also valid for ϕ production via decays of intermediate nonstrange baryon resonances. In addition, besides the sensitivity to the excitation of s-channel baryon resonances, ϕ meson production is an excellent channel to study subprocesses underlying the photoproduction of vector mesons in general.

The ϕ production mechanism depends on the four-momentum transfer $t = (P_\gamma - P_\phi)^2$, where P_γ and P_ϕ are the four-momenta of the incoming photon and the outgoing ϕ meson. At low t the reaction $\gamma p \to \phi p$ can be diffractive and proceed with Pomeron exchange and suppressed π and η exchange, while the contribution of π and η exchange diagrams, as well as production of the ϕ via decay of excited intermediate baryon resonances, are more relevant at higher values of t [16–19]. However, no information on the coupling of baryon resonances to this channel is presently available [20].

Until now the ϕ photoproduction cross section has only been measured in a very limited kinematic range and only for the charged decay mode, $\phi \to K^+K^-$ [21–28]. The SAPHIR [21] and LEPS [22] data appear to show a peak in the cross section at about $1.8 \leqslant E_\gamma \leqslant 2.4$ GeV photon beam energy range, as presented in Fig. 1. In contrast, the calculation of Titov and Lee [16] is smoothly increasing over this range.

Recently, Ryu *et al.* [29] argued that coupled-channel interactions may be responsible for the observed local enhancement of the forward cross section in a model-dependent way. The main reason for this is the proximity of the energy threshold of two processes, $\gamma p \to K^+\Lambda(1520)$ and $\gamma p \to \phi p$. Therefore, the first intermediate process may affect the observed cross section of the second one owing to the final state (or coupled-channel) interaction.

An alternative explanation of the nonmonotonic energy dependence of the forward cross section is proposed in Ref. [14], where the authors interpret the existence of the bump in the differential cross sections at forward angles and near the reaction threshold as being attributable to an excitation of missing nucleon resonances with a non-negligible strangeness content.

Equally interestingly, at certain energies ϕ production and baryon production can also interfere. The $\gamma p \to p\phi \to pK\bar{K}$ reaction can interfere with the $\gamma p \to BK \to pK\bar{K}$ reaction [where B is a baryon resonance that can decay to $pK(\bar{K})$] because both have the same final state. For example, the final state pK^-K^+ can result from either ϕ photoproduction in the charged decay channel or from production of a K^+ and a prominent $\Lambda(1520)$ hyperon resonance with subsequent decay to pK^-. However, if this is the case, then the photoproduction cross section associated with the pK_SK_L final state in the neutral decay mode $\phi \to K_SK_L$ should differ from the charged decay mode as there is no similar prominent meson-baryon production mechanism in this case.

The analysis of ϕ photoproduction in the neutral decay channel is therefore a powerful tool to achieve a deeper

*Corresponding author; mamaryan@odu.edu
†Current address: Christopher Newport University, Newport News, VA 23606, USA.
‡Current address: Los Alamos National Laboratory, Los Alamos, NM 87544, USA.
§Current address: Skobeltsyn Nuclear Physics Institute, 119899 Moscow, Russia.
‖Current address: Institut de Physique Nucléaire ORSAY, Orsay, France.

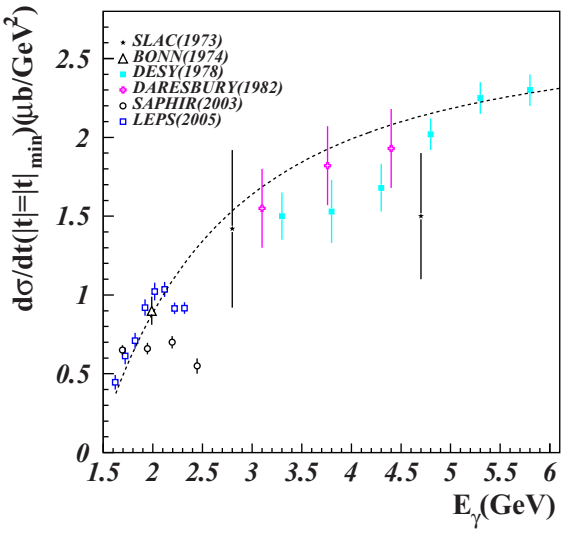

FIG. 1. (Color online) Measured ϕ photoproduction cross section for the charged kaon decay channel ($d\sigma/dt$), extrapolated to $t = t_{\min}$, as a function of incident photon energy E_γ [22]. The dashed line shows the cross section calculated according to the model of Titov and Lee [16].

understanding of the underlying photoproduction mechanisms. The high-statistics CLAS data allow a measurement of the photoproduction cross section of the ϕ meson in this decay mode over a wide kinematic range.

II. EXPERIMENT

The present analysis is based on the g11a data set collected in 2004 using the CLAS detector at the Thomas Jefferson National Accelerator Facility (Jefferson Lab) [30]. The experiment was performed using a photon beam produced through bremsstrahlung from an electron beam of energy 4.02 GeV. A scintillator hodoscope system combined with a dipole magnet was used to tag the photon time and energy in the range of 0.8 to 3.8 GeV with a resolution of 0.1% of the incident electron energy [31]. The photon timing resolution was 120 ps. In this experiment the photon beam was incident on a 40-cm-long liquid hydrogen target, centered 10 cm upstream from the center of the CLAS detector. The integrated luminosity was approximately 80 pb^{-1}.

A segmented scintillator detector (the Start Counter) surrounding the target was used for timing and triggering purposes [32]. Particles from the reaction were detected in the CLAS detector, consisting of six identical sectors, equipped with time-of-flight (TOF) scintillator counters [33], electromagnetic calorimeters [34], drift chambers [35–38], and Čerenkov counters [39], covering nearly 4π solid angle. The drift chambers consisted of three regions, located at three radial locations in each of the six sectors. The first region was placed before the strong magnetic field region, the second region was placed inside of a toroidal magnetic field used for momentum analysis, and the third region was placed after the magnetic field. The momentum resolution of the CLAS detector is momentum dependent and is of the order of $\Delta P/P \sim 0.5\%$. Charged-particle identification is based on simultaneous measurement of their momenta and TOF. Owing to various misalignments of the photon tagging system components, the measured photon energy had some inaccuracies causing reconstructed particle masses to deviate from their correct values. The momenta of detected particles also had inaccuracies because of the energy loss during their flight through the target and detectors. The discrepancies in the toroidal magnetic field map and in drift-chamber survey information were causing some deviations in reconstructed particle momenta. To correct these inaccuracies, photon beam energy and charged-particle momentum corrections were applied to data. The raw data used in this analysis were processed in the same way as in Ref. [40], including corrections for the energy loss of charged particles in the target, uncertainties in the magnetic field, and misalignments of the drift chambers.

III. DATA ANALYSIS

A. Reconstruction of the final state

To select the desired final state, we required that the events contained only three reconstructed charged particles in the final state: a proton, π^+, and π^-. These particles were identified by the standard CLAS event reconstruction software. The particle identification was based on the difference between the measured velocity β_{meas} of the detected particle and the expected velocity β_{th} calculated from the measured momentum and the masses of the different particles. The particle type was chosen based on the minimum difference between the measured β_{meas} and β_{th} velocities.

The start time of the event at the interaction vertex was determined using the rf signal from the accelerator injector that defined the timing of the electron bunches in the beam. The correct bunch containing the original electron that produced the interacting photon was selected by matching the timing information from the tagger counters and the CLAS Start Counter. Figure 2 shows the distribution of the difference between the times from the best matching Start Counter hit and the time of all hits in the photon tagger in the event. The 2-ns structure corresponds to the bunch spacing of the

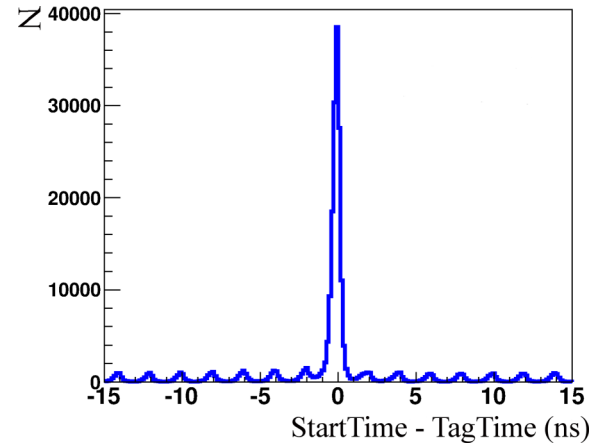

FIG. 2. (Color online) Difference between the time of the Start Counter hit closest to the event start time and the time of the tagger hits. A ±2-ns cut was used to select good photons.

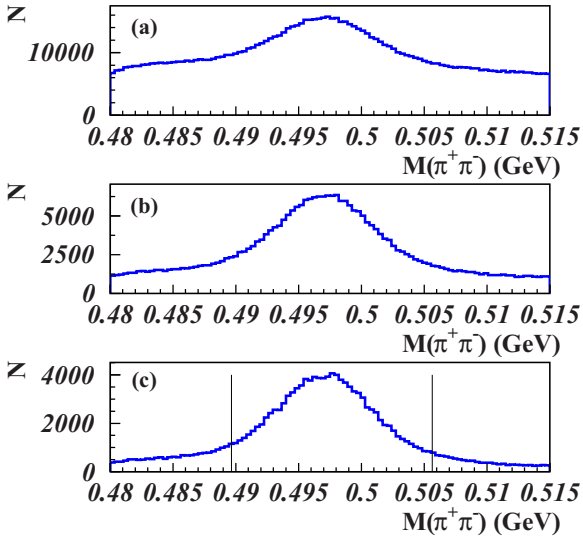

FIG. 3. (Color online) Invariant mass of the $\pi^+\pi^-$ system from the $\gamma p \to p\pi^+\pi^-$ reaction: (a) with a cut on the mass of the missing K_L from the $\gamma p \to p\pi^+\pi^- X$ reaction $|M_X - M_{K_L}| < 0.1$ GeV; (b) with a cut on the mass of the missing K_L from the $\gamma p \to p\pi^+\pi^- X$ reaction $|M_X - M_{K_L}| < 0.015$ GeV; (c) with the previous cut and an additional cut on the missing mass of $\gamma p \to pX$, $|M_X - M_\phi| < 0.02$ GeV.

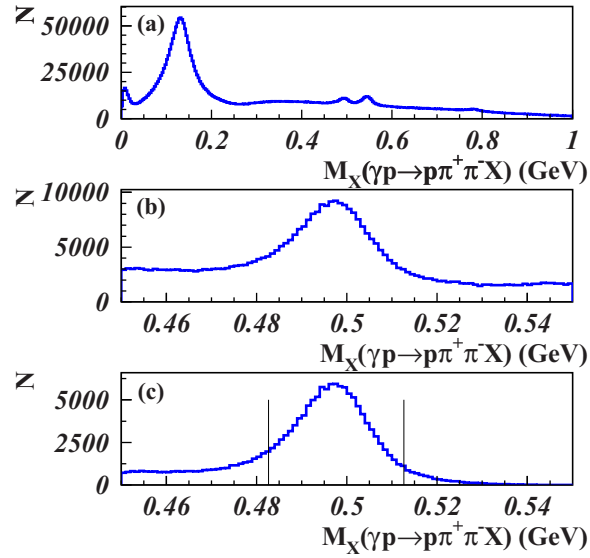

FIG. 4. (Color online) Missing mass of the $\gamma p \to p\pi^+\pi^- X$ reaction: (a) with a cut on the invariant mass of the $\pi^+\pi^-$ system in the $\gamma p \to p\pi^+\pi^-$ reaction $|M(\pi^+\pi^-) - M_{K_S}| < 0.035$ GeV; (b) with a cut on the invariant mass of $\pi^+\pi^-$ $|M(\pi^+\pi^-) - M_{K_S}| < 0.008$ GeV; (c) with the previous cut and an additional cut on the missing mass of $\gamma p \to pX$, $|M_X - M_\phi| < 0.02$ GeV.

electrons in the CEBAF beam that were designated for Hall B extraction. To suppress the accidental coincidences from the different beam bunches, we apply a cut on the time difference |Tag Time − Start Time| < 2 ns. We also required that events contain only one photon detected in the photon tagging system within this -ns time interval.

The momenta for protons and pions were required to be $P_\pi > 0.1$ GeV and $P_p > 0.35$ GeV, respectively, to avoid momentum values where charged track reconstruction becomes problematic. The minimum momentum cuts eliminate a very small fraction of pions (about 0.4%) and protons (about 3%) in our selected event sample.

K_S mesons are reconstructed using the invariant mass $M(\pi^+\pi^-)$ of the $\pi^+\pi^-$ system. Because the mean lifetime of the K_L mesons is about 50 ns, few K_L decayed in the CLAS detector. Thus, K_L particles were reconstructed from the missing mass of the detected particles in the $\gamma p \to p\pi^+\pi^- X$ reaction as $M_X^2 = (P_\gamma + P_t - P_{\pi^+} - P_{\pi^-} - P_p)^2$, where P_i are the four momenta of the photon, target proton, detected π^+ and π^-, and proton, respectively. The missing mass of the $\gamma p \to pX$ system was used to select events coming from the decay of the ϕ meson.

To suppress the background under the ϕ meson, cuts were applied to the following distributions:

(i) invariant mass $M(\pi^+\pi^-)$ of the $\pi^+\pi^-$ system;
(ii) missing mass M_X of the $\gamma p \to p\pi^+\pi^- X$ reaction.

Figure 3 shows the invariant mass of the $\pi^+\pi^-$ system with wide and narrow cuts on M_{K_L} and with a cut on M_ϕ. $M(\pi^+\pi^-)$ is required to be within 2σ of the K_S mass, $|M(\pi^+\pi^-) - M_{K_S}| \leqslant 0.008$ GeV.

Figure 4 shows the mass distribution of the missing K_L in the $\gamma p \to \pi^+\pi^- pX$ reaction with wide (8σ) and narrow (2σ) cuts on the K_S mass and with a cut on M_ϕ. To select K_L, a cut was applied on the missing mass $M_X(\gamma p \to p\pi^+\pi^- X)$ to be within 2σ of the K_L mass: $|M_X - M_{K_L}| \leqslant 0.015$ GeV.

Figure 5 shows the distribution of the missing mass of the $\gamma p \to pX$ reaction, where ϕ production is visible

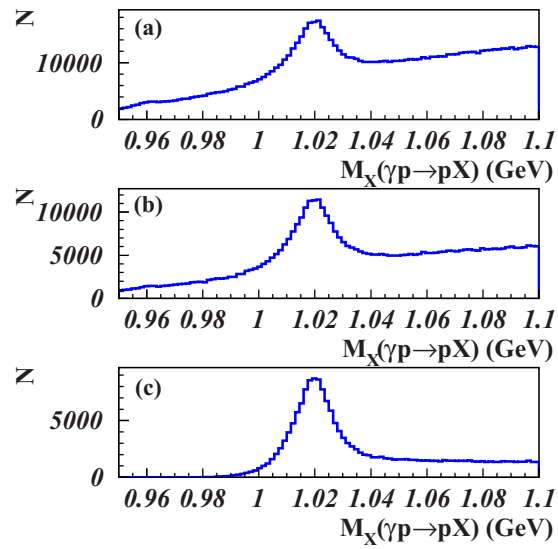

FIG. 5. (Color online) The missing mass of the $\gamma p \to pX$ reaction: (a) with cuts on the invariant mass of $\pi^+\pi^-$ $|M(\pi^+\pi^-) - M_{K_S}| < 0.035$ GeV and on the mass of the missing K_L from the $\gamma p \to p\pi^+\pi^- X$ reaction $|M_X - M_{K_L}| < 0.1$ GeV; (b) with a cut on the invariant mass of $\pi^+\pi^-$ $|M(\pi^+\pi^-) - M_{K_S}| < 0.008$ GeV; (c) with the previous cut and an additional cut on the mass of the missing K_L from the $\gamma p \to p\pi^+\pi^- X$ reaction $|M_X - M_{K_L}| < 0.015$ GeV.

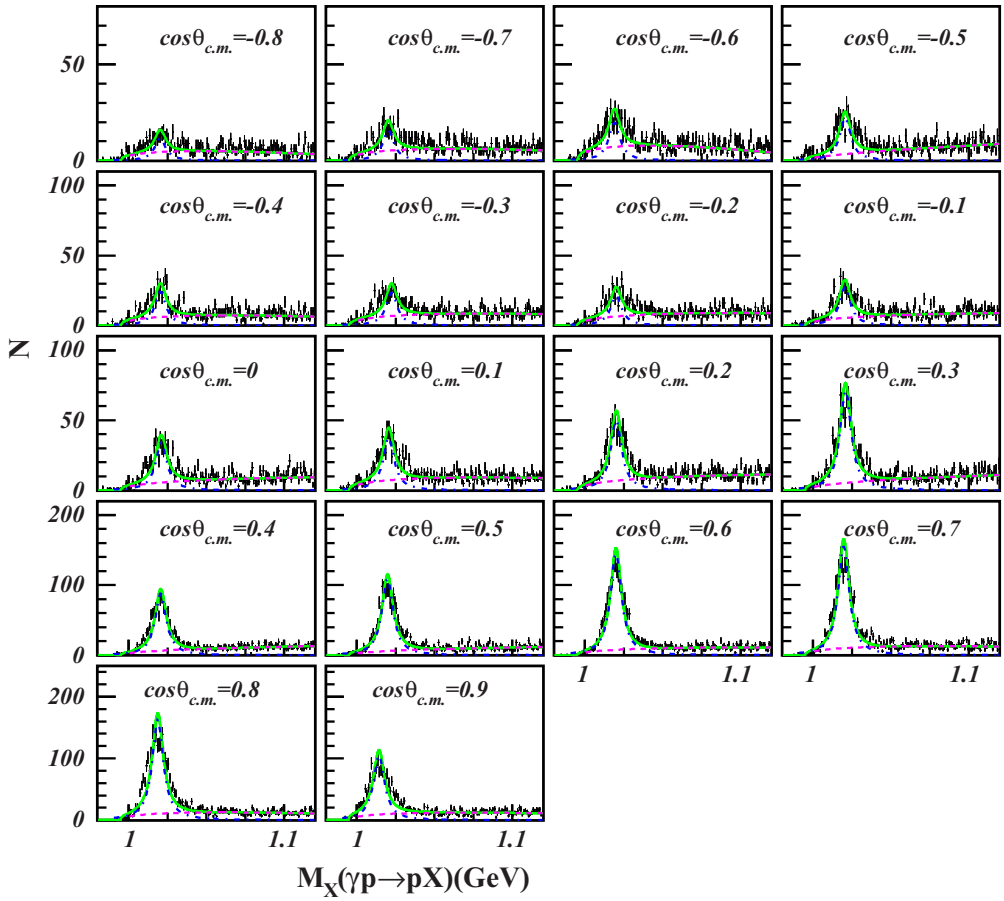

FIG. 6. (Color online) Signal and background separation for $1.8 \leqslant E_\gamma < 2.0$ GeV and different $\cos\theta_{\mathrm{c.m.}}$ bins. The histograms (black) are the unweighted distributions from data. The dash-dotted line (blue) shows the signal from the fit. The dashed line (magenta) shows the background from the fit. The solid line (green) shows the overall fit of the mass distribution.

through the prominent peak at around 1.02 GeV, after cuts: (a) $|M(\pi^+\pi^-) - M_{K_S}| < 0.035$ GeV and $|M_X - M_{K_L}| < 0.1$ GeV in the reaction $\gamma p \to p\pi^+\pi^- X$; (b) $|M(\pi^+\pi^-) - M_{K_S}| < 0.008$ GeV; (c) $|M(\pi^+\pi^-) - M_{K_S}| < 0.008$ GeV and $|M_X - M_{K_L}| < 0.015$ GeV. The signal-to-background ratio improves significantly after all three cuts are applied.

B. Background subtraction

Figure 5 shows that even after the application of the cuts described above there is still visible background left under the ϕ peak. The background is asymmetric, causing simple sideband subtraction techniques to be less reliable for signal-background separation.

Figure 6 shows the fits of $M_X(\gamma p \to pX)$ mass distributions for a given photon energy range and in different $\cos\theta_{\mathrm{c.m.}}$ bins, where $\theta_{\mathrm{c.m.}}$ is the polar angle of the ϕ meson in the center-of-mass system of $\gamma p \to \phi p$. The black points are the experimental data shown with the statistical uncertainties. A Voigt profile, which is a convolution of Lorentzian and Gaussian profiles, was used for the fit of the ϕ signal and to account for the broadening of the signal width owing to the detector resolution effects,

$$S(m,E_\gamma,\zeta) = F(E_\gamma,\zeta)\frac{e^{-\frac{[m-\mu(E_\gamma,\zeta)]^2}{2\sigma^2(E_\gamma,\zeta)}}}{\sigma(E_\gamma,\zeta)}\frac{\Gamma}{[m-\mu(E_\gamma,\zeta)]^2+\Gamma^2}, \tag{1}$$

where Γ is the width of the ϕ, μ is the mean of the ϕ mass distribution, σ is the standard deviation from the mean value for the particular E_γ and $\cos\theta_{\mathrm{c.m.}}$ bin, m is the ϕ mass, $\zeta = \cos\theta_{\mathrm{c.m.}}$, and F is a fit parameter. The Gaussian part of the fit function accounts for the detector resolution impact on the signal width, and the Lorentzian profile describes the natural width of the ϕ. The detector resolution for the mass was allowed to vary in the fit.

The background function used for the fit is of the form

$$B(m,E_\gamma,\zeta) = a(E_\gamma,\zeta)\sqrt{m^2-4m_K^2} + b(E_\gamma,\zeta)\left(m^2-4m_K^2\right), \tag{2}$$

where a and b are obtained from the fit to the data for each bin. Here $m_K = 0.497\,648$ GeV is the mass of a K^0 meson. The total statistics at very backward angles is marginal and extraction of the signal becomes unreliable. Therefore, these kinematic regions were disregarded.

The signal separation for the measurements is done on an event-by-event basis using the fit parameters of the ϕ mass distribution in different E_γ and $\cos\theta_{\text{c.m.}}$ bins to weight each event with the signal probability coefficient defined as

$$W = \frac{S(m,E_\gamma,\zeta)}{S(m,E_\gamma,\zeta)+B(m,E_\gamma,\zeta)}. \quad (3)$$

C. Monte Carlo simulation

To correct the experimental data for acceptance and efficiency, we developed an event generator and used it in conjunction with the simulation of the CLAS detector response. The Monte Carlo (MC) events are generated using the Titov and Lee theoretical model for ϕ photoproduction [16], which describes well the existing data for $1.6 < E_\gamma < 3.6$ GeV and for the range of $t = (P_\gamma - P_\phi)^2$ covered by this experiment. The ϕ then decays as follows: $\phi \to K_S + K_L$ and $K_S \to \pi^+\pi^-$. The simulated final state of $p\pi^+\pi^-$ is then passed through the GEANT simulation program (GSIM) for the CLAS detector and is processed with the GSIM post processing (GPP) package, which takes into account missing detector channels and finite detector resolution. Finally, all the simulated events are reconstructed using the CLAS standard reconstruction code (RECSIS).

The ϕ decay angular dependencies are taken from the Pomeron exchange model of Titov and Lee [16]. The t dependence of the ϕ production is parametrized by the exponential form with $I \sim e^{-B(t-t_{\text{min}})}$, with a constant slope of $B = 3.4$ GeV^{-2}.

The MC events were generated using uniform photon energy distribution. The photon energy dependence was determined by fitting the reconstructed simulated events to the experimental yield.

The detector acceptance correction factor, here also referred to as acceptance correction, is obtained for every E_γ and $\cos\theta_{\text{c.m.}}$ bin as the ratio of the number of reconstructed events to the number of simulated events. The relative uncertainty of the acceptance correction is estimated on a bin-by-bin basis by assuming a binomial distribution for the detection and reconstruction probability and using the following expression:

$$\sigma_{\text{Acc}} = \sqrt{\frac{\left(1-\frac{R}{N}\right)}{\frac{R}{N}(N-1)}}, \quad (4)$$

where N is the total number of simulated events and R is the number of accepted events. The average uncertainties owing to the acceptance corrections are on the order of ≈5% and are included into the statistical uncertainty of the measured values on a bin-by-bin basis.

D. Fiducial cuts

Both the experimental data and the detector acceptance were binned in two dimensions: the incident photon energy E_γ and either $\cos\theta_{\text{c.m.}}$ or $|t - t_{\text{min}}|$. The cross sections were averaged over the azimuthal angle. The bin sizes of the data and acceptance lookup tables were the same. To avoid the areas at the edges of the CLAS kinematic coverage, where our detector simulation did not reliably reproduce the experimental data, we developed a cut to eliminate those data bins. First, we found the t bin with maximal value of acceptance for each energy bin. Next, we eliminated all t bins where the acceptance value was estimated to be less than 12% from its maximal value for the same energy bin.

For this analysis the proton, π^+, and π^- detection efficiencies were obtained using two reactions: $\gamma p \to p\pi^+\pi^-$ and $\gamma p \to p\pi^+\pi^-\pi^+\pi^-$. Events were selected based on complete exclusivity; in case one particle was missed it was reconstructed by missing mass. The efficiencies were obtained as a function of the θ and ϕ angles and momenta of the detected particles in the laboratory frame. We only used these efficiency values for cuts and did not apply them to the data because the detector inefficiencies were already accounted for by using the GSIM and GPP package (Sec. III C). More details about the detection efficiency in this analysis can be found in Ref. [41].

The fiducial cuts were applied to eliminate regions of the detector where the particle detection and reconstruction efficiency changed rapidly and was less than 40%. Additionally, events with kinematics corresponding to malfunctioning TOF scintillator paddles were excluded. These two cuts were applied both to data and to MC reconstructed events.

E. Normalization

The differential cross sections are calculated using

$$\frac{d\sigma}{dt} = \left[\frac{A}{\mathcal{F}(E_\gamma)\rho L N_A}\right]\frac{\mathcal{Y}(E_\gamma,t-t_{\text{min}})}{\Delta(t-t_{\text{min}})\eta(E_\gamma,t-t_{\text{min}})} \times \frac{1}{BR(\phi \to K_sK_L).} \quad (5)$$

Here A, ρ, and L are the atomic weight, density, and the length of the target, respectively. N_A is Avogadro's number and $\mathcal{F}(E_\gamma)$ is the total number of photons incident on the target in that photon energy bin. $\Delta(t - t_{\text{min}}) = 0.04$ GeV^2 is the $t - t_{\text{min}}$ bin size. BR ≈ 0.342 [20] is the branching ratio for the decay $\phi \to K_SK_L$. $\mathcal{Y}(E_\gamma,t - t_{\text{min}})$ is the number of events in the given photon energy and $t - t_{\text{min}}$ bin, that passed all cuts (see Table I) after the background separation (see Sec. III B). $\eta(E_\gamma,t - t_{\text{min}})$ is the acceptance in the $(E_\gamma,t - t_{\text{min}})$ bin. The cross sections $d\sigma/d\cos\theta_{\text{c.m.}}$ was obtained in the same way as a function of $\cos\theta_{\text{c.m.}}$ using the corresponding yields and acceptance correction factors and the $\cos\theta_{\text{c.m.}}$ bin size of 0.1.

The photon flux for the experiment was obtained using the CLAS GFLUX software package [42]. In the g11a experiment a

TABLE I. Table of cuts applied for data selection.

Cuts	Description
Momentum cuts	$P_{\pi^+,\pi^-} > 0.1$ GeV, $P_p > 0.35$ GeV
K_S selection	$\lvert M(\pi^+\pi^-) - 0.497\,65\rvert \leqslant 0.008$ GeV
K_L selection	$\lvert M_X(p\pi^+\pi^-) - 0.497\,65\rvert \leqslant 0.015$ GeV
Efficiency cut	$\mathcal{E}_{p,\pi^+,\pi^-} > 40\%$
TOF paddles	Malfunctioning TOF paddles
Fiducial cuts	Sec. III D
Timing cut	$\lvert \text{TAG}_{\text{time}} - \text{ST}_{\text{time}}\rvert < 2$ ns
Acceptance cuts	$\eta/\eta_{\text{max}} > 12\%$

TABLE II. Summary of systematic uncertainties.

Uncertainty source	Uncertainty (%)
Background subtraction	10
Photon normalization	7.7 [44]
Particle detection efficiency cut	2–6
Current-dependent correction	3 [45]
$\phi \to K_L K_S$ branching fraction	0.6 [20]
Photon transmission efficiency	0.5 [44]
Target length	0.13
Target density	0.11 [45]

linear dependence of the normalized photon yield on the beam current was observed. This was suggested to be attributable to the malfunctioning of the hardware used to estimate the data acquisition live time. A correction factor was obtained fitting the yield dependence on the beam current with a line and correcting for the drop in the normalized yield. This factor was 1.187 at the electron beam current of 65 nA [43].

As mentioned in Sec. III A, it was required to have only one photon present in the tagger within the $\pm$2-ns time interval between the tagger and the Start Counter: $|\mathrm{TAG_{time}} - \mathrm{ST_{time}}| < 2$ ns. This cut removed some good events from the data. This loss of events was corrected for by normalizing the overall yield with two correction factors: *multiple hits* and *time window*. The *multiple hits* correction was found to be on the order of 18% for our process and was obtained by comparison of the ϕ meson yields with and without the requirement to have only one good photon detected by the tagger for the event. The 6% *time window* correction is obtained by comparing the yields with $\Delta t = 2$ ns cut and with $\Delta t = 15$ ns (no cut) [43].

F. Systematic uncertainties

The summary of the estimated relative systematic uncertainties of the measured cross sections is given in Table II.

As described in Sec. III B, the ϕ meson background was estimated from the fits of the ϕ mass distributions in each photon energy and $\cos\theta_{\mathrm{c.m.}}$ bin. The systematic uncertainty owing to background subtraction was estimated from the uncertainties of the fit parameters and in average was on the order of 10%.

To eliminate low-efficiency regions of the detector a cut was applied on the single-particle detection efficiencies. This cut was applied to both the reconstructed MC events and the data (see Sec. III D). The systematic uncertainty of this cut was estimated by measuring the acceptance-corrected cross sections for three different efficiency cuts: 30%, 35%, and 40%. The systematic uncertainty was estimated bin by bin as the standard deviation of the three resulting cross sections. The average systematic uncertainty owing to the efficiency cut was about 6%.

In the previous section we described a correction factor owing to the beam current dependence of the normalized yield for the g11a experiment. This factor was obtained by a fit and has an uncertainty of about 3%.

The photon flux normalization uncertainty of 7.7% was obtained from comparison of the cross sections for a set of reference reactions ($K^+\Lambda$, $p\omega$, $p\eta$) measured using the current (g11a) data set and other experimental data [44,46,47].

The overall systematic uncertainty of the differential cross section averaged over all bins is about 14%.

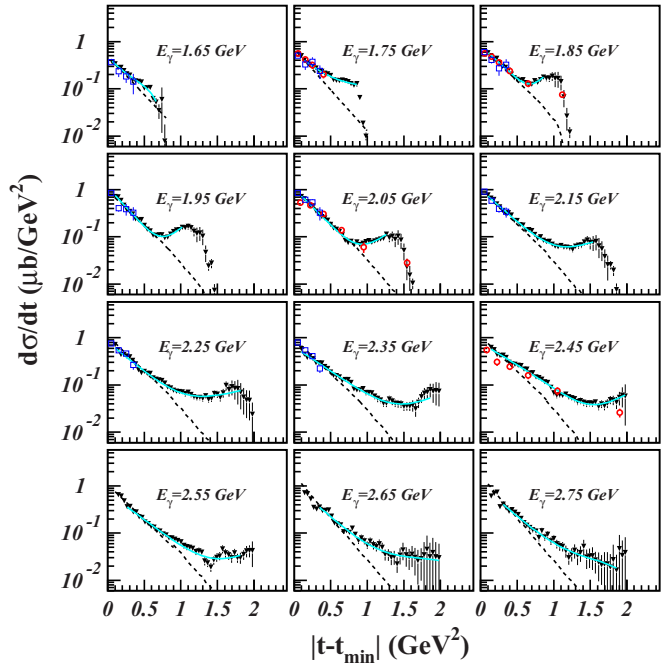

FIG. 7. (Color online) Differential cross section $d\sigma/dt$ plotted versus $|t - t_{\mathrm{min}}|$ for different photon energy bins in the $1.6 \leqslant E_\gamma < 2.8$ GeV range. The solid downward triangles (black) are the results of the current CLAS(2013) analysis for the neutral decay mode of the ϕ. The open circles (red) are the SAPHIR [21] data for the charged-mode topology. The open squares (blue) are the LEPS [22] data for the charged-mode topology. The solid lines (cyan) show the fit function. The dashed lines (black) show the MC distribution.

IV. EXPERIMENTAL RESULTS

The differential cross section for ϕ meson photoproduction was measured as a function of $|t - t_{\mathrm{min}}|$ and $\cos\theta_{\mathrm{c.m.}}$ for different photon energy bins. The differential cross section $d\sigma/dt$ was also measured as a function of E_γ for different $\cos\theta_{\mathrm{c.m.}}$ bins.

A. The t dependence

The differential cross sections $d\sigma/dt$ were obtained for different four-momentum transfer $t - t_{\mathrm{min}}$ bins and for 0.1-GeV photon energy bins in the photon energy range 1.6–3.6 GeV. Corresponding data tables are presented in Tables III-XI.

Figures 7 and 8 show the $|t - t_{\mathrm{min}}|$ dependencies of the differential cross section for different photon energy bins. The world data for the charged decay channel are also included for comparison. The neutral decay mode data are fitted with an exponential function (solid lines) to obtain the differential cross section at $t = t_{\mathrm{min}}$ and the slope of the t dependence of ϕ photoproduction. These measurements show that in addition to the fast exponential falloff, which is characteristic of t-channel exchange, at the higher values of the photon beam energy

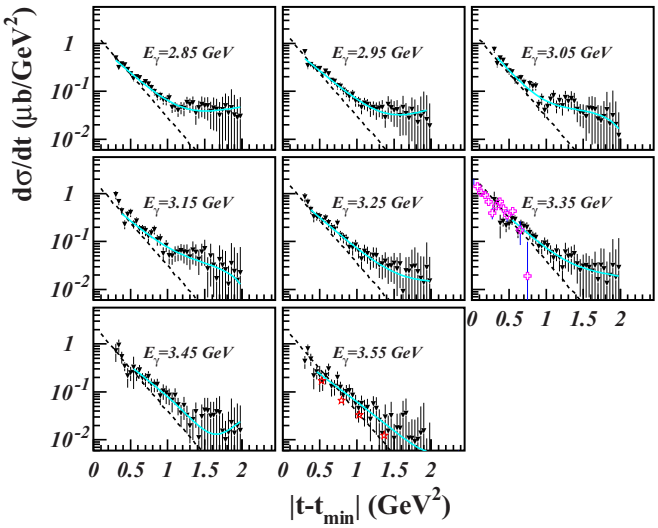

FIG. 8. (Color online) Differential cross section $d\sigma/dt$ plotted versus $|t - t_{\rm min}|$ for different photon energy bins in the $2.8 \leqslant E_\gamma \leqslant 3.6$ GeV range. The solid triangles (black) are the results of the current CLAS(2013) analysis for the neutral decay mode of the ϕ. The open crosses (magenta) are the DARESBURY [23] data for the charged mode. The open stars (red) represent the CLAS(2000) [27] results for charged decay mode of the ϕ meson. The solid lines (cyan) show the fit function. The dashed lines (black) show the MC distribution.

(about 2 GeV) the cross section distribution starts flattening at larger values of t. This is indicative of the possible presence of other mechanisms of ϕ production, such as excitation and decay of intermediate nucleon resonances [19].

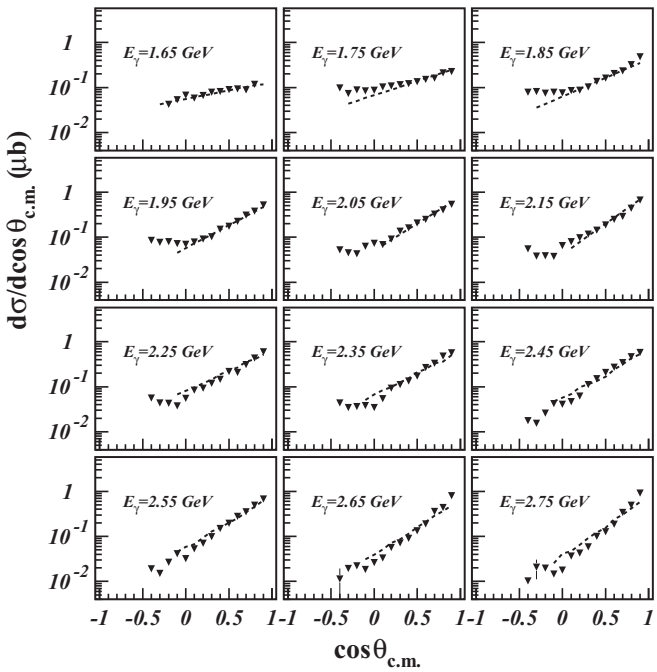

FIG. 9. The $\cos\theta_{\rm c.m.}$ dependence of the ϕ meson differential cross section $d\sigma/d\cos\theta_{\rm c.m.}$ for different photon beam energy bins $1.6 \leqslant E_\gamma < 2.8$ GeV. The $\cos\theta_{\rm c.m.}$ bin size is 0.1. The dashed lines (black) show the MC distribution.

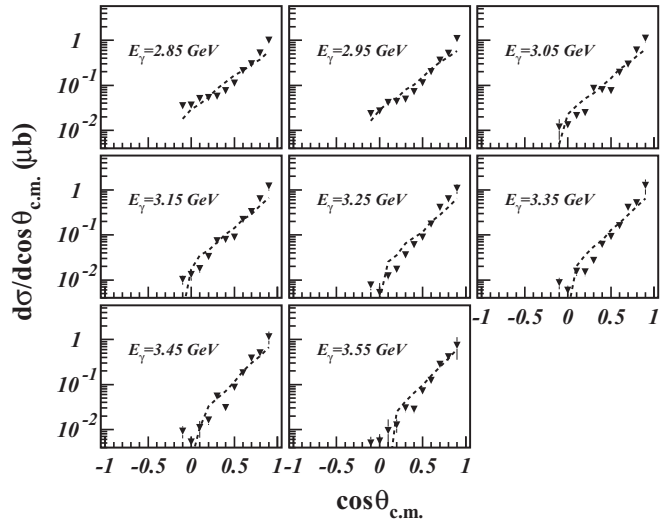

FIG. 10. The $\cos\theta_{\rm c.m.}$ dependence of the ϕ meson differential cross section $d\sigma/d\cos\theta_{\rm c.m.}$ for different photon beam energy bins $2.8 \leqslant E_\gamma \leqslant 3.6$ GeV. The $\cos\theta_{\rm c.m.}$ bin size is 0.1. The dashed lines (black) show the MC distribution.

Figures 9 and 10 show the differential cross section $d\sigma/d\cos\theta_{\rm c.m.}$ plotted as a function of $\cos\theta_{\rm c.m.}$. The results are plotted for 0.1-GeV photon energy bins. Corresponding data tables are presented in Tables XII-XV.

B. The E_γ dependence

For this work, the differential cross section $d\sigma/dt$ for the process will be given as

$$\frac{d\sigma}{dt} = \frac{1}{2}\left(\frac{1}{E_\gamma|\vec{p}_{\,\phi}|}\right)_{\rm c.m.}\left(\frac{d\sigma}{d\cos\theta_{\rm c.m.}}\right). \qquad (6)$$

Figures 11 and 12 show the E_γ dependence of the differential cross section $d\sigma/dt$ in different $\cos\theta_{\rm c.m.}$ bins. $d\sigma/dt$ is measured at different photon energies E_γ (for 0.05-GeV-wide bins of E_γ).

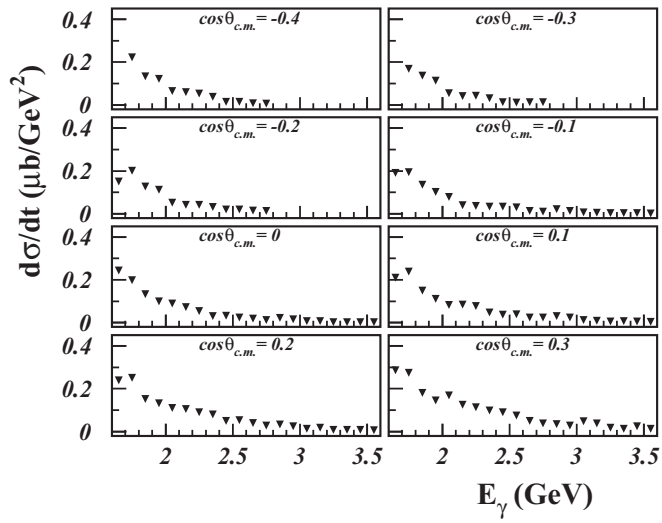

FIG. 11. The E_γ dependence of the ϕ meson differential cross section $d\sigma/dt$ in different $\cos\theta_{\rm c.m.}$ bins for $-0.45 \leqslant \cos\theta_{\rm c.m.} < 0.35$.

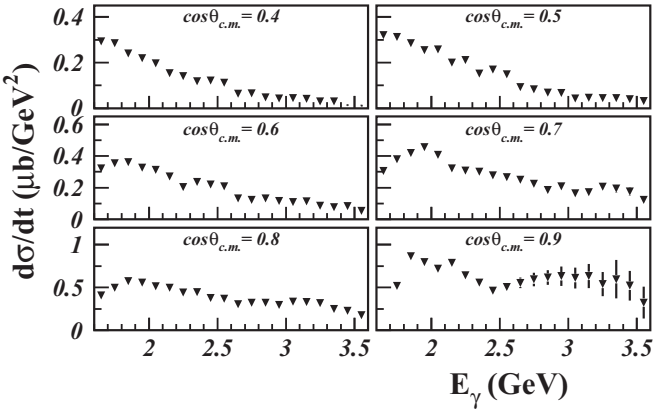

FIG. 12. The E_γ dependence of the ϕ meson differential cross section $d\sigma/dt$ in different $\cos\theta_{\rm c.m.}$ bins for $0.35 \leqslant \cos\theta_{\rm c.m.} < 0.95$.

In forward angle $\cos\theta_{\rm c.m.}$ bins, corresponding to the low-t region, there appears to be a local enhancement in $d\sigma/dt$ in the range of $2.0 < E_\gamma < 2.4$ GeV and a maximum at about $E_\gamma \approx 2.2$ GeV. In this angular region, at higher energies ($E_\gamma >$ 2.6 GeV) the cross section behavior is almost constant, as expected by Pomeron exchange mechanism dominance in ϕ production [16].

C. Total cross section

To determine the total cross section, an exponential function of the form $Ae^{-B|t-t_{\rm min}|} + P(3)$, where $P(3)$ is a third-order polynomial function, is used to fit the $|t - t_{\rm min}|$ dependence of the differential cross section $d\sigma/dt$. The fit range was selected to have the χ^2/ndf value closest to 1. The extracted values of the differential cross section at $t = t_{\rm min}$ and the t slope from the fit depend on the range of the fit and vary within 10%. The higher t regions, where the cross section increases and deviates from the exponential behavior, were not included in the fit. Figures 13(a) and 13(b) show the total cross section and the B slopes for the different photon energy bins, respectively. The total cross section still has some enhancement in the photon beam energy range of about 1.8–2.3 GeV just as observed in the charged-mode decay. The photon beam energy dependence of the slope of the t distribution also has some local structure in the photon beam energy range of 1.8–2.3 GeV. Corresponding data tables are summarized in Table XVI.

V. CONCLUSIONS

Differential cross sections for photoproduction of the ϕ meson via its neutral decay channel in the reaction $\gamma p \to p\phi(K_S K_L)$ have been measured for the first time. The t dependence of the cross section at fixed photon energy indicates that the mechanism of ϕ production deviates from an exponential behavior at higher values of t. Detailed model calculations will be required to estimate the relative contribution to the ϕ production stemming from Pomeron, π, and η exchanges. The presented data will help to constrain the contribution of intermediate s-channel nucleon resonances and final-state interactions.

However, the energy dependence of the differential cross section at the forward limit shows a similar local maximum as was observed previously in photoproduction of the ϕ meson in the charged decay mode. There are different explanations for this local maximum based on either coupled-channel effects, excitation of intermediate nucleon resonances, or interference with $\Lambda(1520)$ production as was proposed in Refs. [14,17,18,29].

A full understanding of the mechanism of ϕ photoproduction at low energy and especially the energy dependence of the forward cross sections will require systematic comparison of theoretical model predictions with experimental data. Theoretical models for this purpose should include not only the ϕ photoproduction in both decay modes, but also the photoproduction cross sections of associated $pK(\bar{K})$ system as meson-baryon final states are significantly different in these two decay modes.

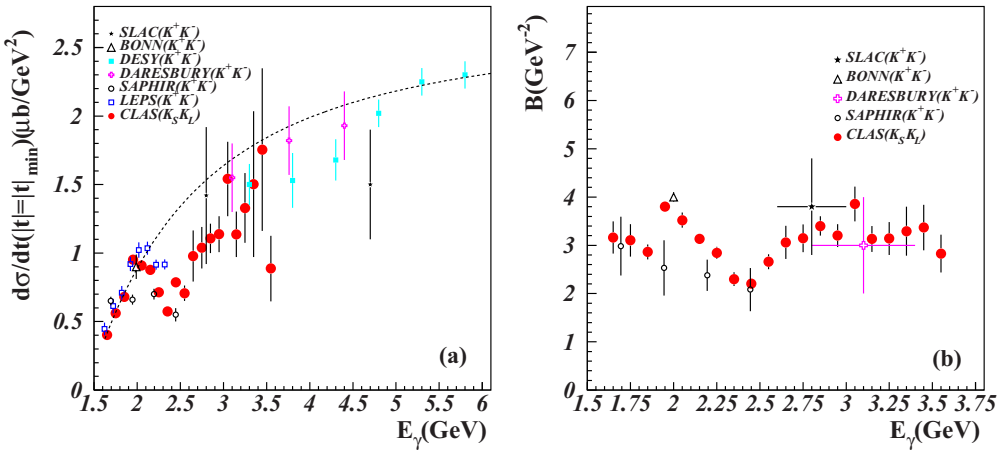

FIG. 13. (Color online) (a) Differential cross section $d\sigma/dt$ at $t = t_{\rm min}$ and (b) ϕ meson photoproduction slope B for the neutral decay mode plotted as a function of the photon beam energy E_γ. The error bars represent the statistical uncertainties. The solid circles (red) are the current CLAS (2013) data in the neutral mode. For the charged decay mode, the open circles (black) are the SAPHIR [21] results, the open squares (blue) are the LEPS [22] results, the open crosses (magenta) are the DARESBURY [23] data, the stars (black) are the SLAC [24] data, the open upward triangles (black) are the BONN [25] data, and the solid squares (cyan) are the DESY [26] data. The dashed curve represents the prediction of a model including the Pomeron trajectory, π, and η exchange processes [16].

ACKNOWLEDGMENTS

We would like to acknowledge the outstanding efforts of the staff of the Accelerator and the Physics Divisions at Jefferson Lab that made the experiment possible. This work was supported in part by the Italian Istituto Nazionale di Fisica Nucleare, the French Centre National de la Recherche Scientifique and Commissariat à l'Energie Atomique, the United Kingdom's Science and Technology Facilities Council (STFC), the US Department of Energy and National Science Foundation, and the Korea Science and Engineering Foundation. The Southeastern Universities Research Association (SURA) operates the Thomas Jefferson National Accelerator Facility for the United States Department of Energy under Contract No. DEAC05-84ER40150.

APPENDIX A

The following data tables include measured differential cross section $d\sigma/dt$ for different $|t - t_{\min}|$ and photon beam energy values.

TABLE III. $d\sigma/dt$ (μb/GeV^2) vs $|t - t_{\min}|$ (GeV^2) for different photon beam energies. Superscripts are statistical errors and subscripts are systematic errors.

E_γ (GeV)	$\sqrt{s}$ (GeV)	$\lvert t - t_{\min}\rvert$ (GeV^2)				
		0.060	0.100	0.140	0.180	0.220
1.6500	1.9942	$0.3367^{\pm 0.0168}_{\pm 0.0677}$	$0.2808^{\pm 0.0133}_{\pm 0.0385}$	$0.2853^{\pm 0.0135}_{\pm 0.0103}$	$0.2411^{\pm 0.0119}_{\pm 0.0173}$	$0.2059^{\pm 0.0108}_{\pm 0.0104}$
1.7500	2.0407	$0.5033^{\pm 0.0210}_{\pm 0.0331}$	$0.4052^{\pm 0.0154}_{\pm 0.0385}$	$0.3562^{\pm 0.0138}_{\pm 0.0298}$	$0.3262^{\pm 0.0130}_{\pm 0.0189}$	$0.2929^{\pm 0.0115}_{\pm 0.0218}$
1.8500	2.0861	$0.5815^{\pm 0.0252}_{\pm 0.0682}$	$0.4991^{\pm 0.0196}_{\pm 0.0443}$	$0.4159^{\pm 0.0156}_{\pm 0.0495}$	$0.4453^{\pm 0.0169}_{\pm 0.0701}$	$0.3571^{\pm 0.0145}_{\pm 0.0240}$
1.9500	2.1306	$0.7171^{\pm 0.0361}_{\pm 0.1199}$	$0.7058^{\pm 0.0292}_{\pm 0.0266}$	$0.5945^{\pm 0.0240}_{\pm 0.0471}$	$0.4673^{\pm 0.0195}_{\pm 0.0210}$	$0.3744^{\pm 0.0162}_{\pm 0.0442}$
2.0500	2.1742	$0.7187^{\pm 0.0486}_{\pm 0.1023}$	$0.6419^{\pm 0.0311}_{\pm 0.0344}$	$0.5528^{\pm 0.0255}_{\pm 0.0745}$	$0.4624^{\pm 0.0205}_{\pm 0.0351}$	$0.4505^{\pm 0.0204}_{\pm 0.0307}$
2.1500	2.2170	$0.7754^{\pm 0.0710}_{\pm 0.0604}$	$0.6640^{\pm 0.0415}_{\pm 0.0261}$	$0.6215^{\pm 0.0331}_{\pm 0.0426}$	$0.5022^{\pm 0.0230}_{\pm 0.0248}$	$0.4302^{\pm 0.0212}_{\pm 0.0231}$
2.2500	2.2589	$0.7271^{\pm 0.0846}_{\pm 0.1039}$	$0.5615^{\pm 0.0367}_{\pm 0.0389}$	$0.4425^{\pm 0.0248}_{\pm 0.0408}$	$0.4399^{\pm 0.0269}_{\pm 0.0380}$	$0.4093^{\pm 0.0238}_{\pm 0.0456}$
2.3500	2.3001	$0.5836^{\pm 0.0871}_{\pm 0.0834}$	$0.4521^{\pm 0.0379}_{\pm 0.0204}$	$0.3822^{\pm 0.0275}_{\pm 0.0366}$	$0.4159^{\pm 0.0293}_{\pm 0.0300}$	$0.3583^{\pm 0.0273}_{\pm 0.0192}$
2.4500	2.3405	—	—	—	$0.6228^{\pm 0.0467}_{\pm 0.0316}$	$0.5617^{\pm 0.0400}_{\pm 0.0682}$
2.5500	2.3803	—	—	—	$0.6534^{\pm 0.0536}_{\pm 0.0519}$	$0.6069^{\pm 0.0504}_{\pm 0.1900}$
2.6500	2.4193	—	—	—	$0.7104^{\pm 0.0722}_{\pm 0.0443}$	$0.6868^{\pm 0.0659}_{\pm 0.0301}$
2.7500	2.4578	—	—	—	$0.6062^{\pm 0.0753}_{\pm 0.0371}$	$0.6965^{\pm 0.0733}_{\pm 0.0332}$

TABLE IV. $d\sigma/dt$ (μb/GeV^2) vs $|t - t_{\min}|$ (GeV^2) for different photon beam energies. Superscripts are statistical errors and subscripts are systematic errors.

E_γ (GeV)	$\sqrt{s}$ (GeV)	$\lvert t - t_{\min}\rvert$ (GeV^2)				
		0.260	0.300	0.340	0.380	0.420
1.6500	1.9942	$0.1939^{\pm 0.0107}_{\pm 0.0251}$	$0.1536^{\pm 0.0092}_{\pm 0.0081}$	$0.1456^{\pm 0.0092}_{\pm 0.0076}$	$0.1441^{\pm 0.0101}_{\pm 0.0214}$	$0.1393^{\pm 0.0110}_{\pm 0.0214}$
1.7500	2.0407	$0.2734^{\pm 0.0111}_{\pm 0.0256}$	$0.2335^{\pm 0.0102}_{\pm 0.0099}$	$0.2345^{\pm 0.0113}_{\pm 0.0166}$	$0.2133^{\pm 0.0100}_{\pm 0.0248}$	$0.2082^{\pm 0.0103}_{\pm 0.0124}$
1.8500	2.0861	$0.2992^{\pm 0.0128}_{\pm 0.0438}$	$0.2842^{\pm 0.0122}_{\pm 0.0130}$	$0.2484^{\pm 0.0114}_{\pm 0.0186}$	$0.2034^{\pm 0.0096}_{\pm 0.0236}$	$0.1707^{\pm 0.0087}_{\pm 0.0306}$
1.9500	2.1306	$0.3481^{\pm 0.0159}_{\pm 0.0344}$	$0.3052^{\pm 0.0140}_{\pm 0.0103}$	$0.2398^{\pm 0.0116}_{\pm 0.0184}$	$0.2287^{\pm 0.0119}_{\pm 0.0111}$	$0.2333^{\pm 0.0127}_{\pm 0.0266}$
2.0500	2.1742	$0.3503^{\pm 0.0177}_{\pm 0.0428}$	$0.3038^{\pm 0.0155}_{\pm 0.0244}$	$0.2696^{\pm 0.0146}_{\pm 0.0216}$	$0.2538^{\pm 0.0142}_{\pm 0.0273}$	$0.2266^{\pm 0.0136}_{\pm 0.0154}$
2.1500	2.2170	$0.3629^{\pm 0.0171}_{\pm 0.0175}$	$0.3142^{\pm 0.0150}_{\pm 0.0153}$	$0.3271^{\pm 0.0151}_{\pm 0.0123}$	$0.2915^{\pm 0.0153}_{\pm 0.0134}$	$0.2232^{\pm 0.0133}_{\pm 0.0169}$
2.2500	2.2589	$0.3980^{\pm 0.0236}_{\pm 0.0401}$	$0.3324^{\pm 0.0200}_{\pm 0.0431}$	$0.2801^{\pm 0.0175}_{\pm 0.0170}$	$0.2108^{\pm 0.0130}_{\pm 0.0119}$	$0.1821^{\pm 0.0115}_{\pm 0.0107}$
2.3500	2.3001	$0.2993^{\pm 0.0213}_{\pm 0.0340}$	$0.2929^{\pm 0.0241}_{\pm 0.0295}$	$0.2948^{\pm 0.0189}_{\pm 0.0174}$	$0.2476^{\pm 0.0167}_{\pm 0.0258}$	$0.2237^{\pm 0.0157}_{\pm 0.0390}$
2.4500	2.3405	$0.4452^{\pm 0.0287}_{\pm 0.0388}$	$0.4214^{\pm 0.0275}_{\pm 0.0676}$	$0.4306^{\pm 0.0275}_{\pm 0.0245}$	$0.3818^{\pm 0.0240}_{\pm 0.0336}$	$0.3026^{\pm 0.0210}_{\pm 0.0303}$
2.5500	2.3803	$0.4814^{\pm 0.0346}_{\pm 0.1279}$	$0.3609^{\pm 0.0277}_{\pm 0.0228}$	$0.3652^{\pm 0.0257}_{\pm 0.0290}$	$0.2821^{\pm 0.0214}_{\pm 0.0425}$	$0.2793^{\pm 0.0206}_{\pm 0.0496}$
2.6500	2.4193	$0.5295^{\pm 0.0494}_{\pm 0.0261}$	$0.3505^{\pm 0.0338}_{\pm 0.0150}$	$0.3220^{\pm 0.0306}_{\pm 0.0140}$	$0.3544^{\pm 0.0339}_{\pm 0.0160}$	$0.2980^{\pm 0.0284}_{\pm 0.0154}$
2.7500	2.4578	$0.7359^{\pm 0.0829}_{\pm 0.0339}$	$0.3617^{\pm 0.0384}_{\pm 0.0150}$	$0.4093^{\pm 0.0410}_{\pm 0.0200}$	$0.3380^{\pm 0.0357}_{\pm 0.0138}$	$0.2924^{\pm 0.0313}_{\pm 0.0180}$
2.8500	2.4957	$0.4934^{\pm 0.0515}_{\pm 0.0245}$	$0.3104^{\pm 0.0379}_{\pm 0.0148}$	$0.3718^{\pm 0.0448}_{\pm 0.0209}$	$0.3566^{\pm 0.0392}_{\pm 0.0198}$	$0.2832^{\pm 0.0304}_{\pm 0.0148}$
2.9500	2.5330	$0.6718^{\pm 0.1047}_{\pm 0.0309}$	$0.3422^{\pm 0.0519}_{\pm 0.0180}$	$0.3600^{\pm 0.0466}_{\pm 0.0175}$	$0.3196^{\pm 0.0411}_{\pm 0.0181}$	$0.2948^{\pm 0.0404}_{\pm 0.0146}$
3.0500	2.5698	$0.7510^{\pm 0.1210}_{\pm 0.0503}$	$0.3769^{\pm 0.0651}_{\pm 0.0246}$	$0.4937^{\pm 0.0637}_{\pm 0.0419}$	$0.4405^{\pm 0.0638}_{\pm 0.0294}$	$0.3378^{\pm 0.0488}_{\pm 0.0336}$
3.1500	2.6061	$0.9479^{\pm 0.1849}_{\pm 0.0765}$	$0.6846^{\pm 0.1098}_{\pm 0.0448}$	$0.4364^{\pm 0.0741}_{\pm 0.0288}$	$0.2288^{\pm 0.0477}_{\pm 0.0159}$	$0.3663^{\pm 0.0661}_{\pm 0.0347}$
3.2500	2.6418	$0.8494^{\pm 0.1894}_{\pm 0.0923}$	$0.6616^{\pm 0.1241}_{\pm 0.0579}$	$0.4677^{\pm 0.0921}_{\pm 0.0461}$	$0.3325^{\pm 0.0787}_{\pm 0.0329}$	$0.3453^{\pm 0.0741}_{\pm 0.0323}$
3.3500	2.6771	$0.7554^{\pm 0.3435}_{\pm 0.0679}$	$0.6573^{\pm 0.1652}_{\pm 0.0574}$	$0.2406^{\pm 0.1249}_{\pm 0.0241}$	$0.2626^{\pm 0.0560}_{\pm 0.0289}$	$0.2138^{\pm 0.0564}_{\pm 0.0268}$
3.4500	2.7119	$0.7195^{\pm 0.2952}_{\pm 0.0885}$	$0.9465^{\pm 0.2898}_{\pm 0.0981}$	$0.5407^{\pm 0.1511}_{\pm 0.0586}$	$0.3433^{\pm 0.0745}_{\pm 0.0332}$	$0.2168^{\pm 0.0950}_{\pm 0.0227}$
3.5500	2.7463	$0.4325^{\pm 0.1299}_{\pm 0.0884}$	$0.7958^{\pm 0.1843}_{\pm 0.1106}$	$0.4842^{\pm 0.1374}_{\pm 0.0596}$	$0.2155^{\pm 0.1013}_{\pm 0.0358}$	$0.2609^{\pm 0.0792}_{\pm 0.0314}$

TABLE V. $d\sigma/dt$ (μb/GeV^2) vs $|t - t_{\min}|$ (GeV^2) for different photon beam energies. Superscripts are statistical errors and subscripts are systematic errors.

E_γ (GeV)	$\sqrt{s}$ (GeV)	$\lvert t - t_{\min}\rvert$ (GeV^2)				
		0.460	0.500	0.540	0.580	0.620
1.6500	1.9942	$0.1025^{\pm 0.0093}_{\pm 0.0093}$	$0.1043^{\pm 0.0105}_{\pm 0.0142}$	$0.1058^{\pm 0.0129}_{\pm 0.0137}$	$0.0624^{\pm 0.0094}_{\pm 0.0067}$	$0.0521^{\pm 0.0108}_{\pm 0.0157}$
1.7500	2.0407	$0.1921^{\pm 0.0101}_{\pm 0.0188}$	$0.1556^{\pm 0.0092}_{\pm 0.0093}$	$0.1519^{\pm 0.0096}_{\pm 0.0137}$	$0.1490^{\pm 0.0097}_{\pm 0.0200}$	$0.1535^{\pm 0.0156}_{\pm 0.0131}$
1.8500	2.0861	$0.1575^{\pm 0.0084}_{\pm 0.0179}$	$0.1516^{\pm 0.0082}_{\pm 0.0087}$	$0.1552^{\pm 0.0090}_{\pm 0.0122}$	$0.1350^{\pm 0.0082}_{\pm 0.0224}$	$0.1201^{\pm 0.0074}_{\pm 0.0142}$
1.9500	2.1306	$0.1765^{\pm 0.0100}_{\pm 0.0214}$	$0.1453^{\pm 0.0085}_{\pm 0.0074}$	$0.1341^{\pm 0.0086}_{\pm 0.0315}$	$0.1088^{\pm 0.0073}_{\pm 0.0134}$	$0.1081^{\pm 0.0071}_{\pm 0.0115}$
2.0500	2.1742	$0.1849^{\pm 0.0114}_{\pm 0.0391}$	$0.1535^{\pm 0.0109}_{\pm 0.0088}$	$0.1453^{\pm 0.0107}_{\pm 0.0308}$	$0.1302^{\pm 0.0107}_{\pm 0.0110}$	$0.1100^{\pm 0.0094}_{\pm 0.0118}$
2.1500	2.2170	$0.0754^{\pm 0.0214}_{\pm 0.0088}$	$0.0771^{\pm 0.0272}_{\pm 0.0090}$	$0.0801^{\pm 0.0285}_{\pm 0.0139}$	$0.0647^{\pm 0.0293}_{\pm 0.0112}$	$0.0557^{\pm 0.0249}_{\pm 0.0180}$
2.2500	2.2589	$0.1956^{\pm 0.0138}_{\pm 0.0115}$	$0.1759^{\pm 0.0117}_{\pm 0.0125}$	$0.1774^{\pm 0.0145}_{\pm 0.0131}$	$0.1411^{\pm 0.0115}_{\pm 0.0084}$	$0.1334^{\pm 0.0109}_{\pm 0.0100}$
2.3500	2.3001	$0.1874^{\pm 0.0135}_{\pm 0.0324}$	$0.1606^{\pm 0.0126}_{\pm 0.0149}$	$0.1580^{\pm 0.0118}_{\pm 0.0298}$	$0.1476^{\pm 0.0146}_{\pm 0.0369}$	$0.1252^{\pm 0.0101}_{\pm 0.0086}$
2.4500	2.3405	$0.2775^{\pm 0.0202}_{\pm 0.0193}$	$0.2731^{\pm 0.0195}_{\pm 0.0189}$	$0.2614^{\pm 0.0190}_{\pm 0.0186}$	$0.2566^{\pm 0.0185}_{\pm 0.0208}$	$0.2175^{\pm 0.0158}_{\pm 0.0210}$
2.5500	2.3803	$0.2220^{\pm 0.0180}_{\pm 0.0150}$	$0.2144^{\pm 0.0171}_{\pm 0.0155}$	$0.1710^{\pm 0.0134}_{\pm 0.0268}$	$0.1596^{\pm 0.0126}_{\pm 0.0216}$	$0.1377^{\pm 0.0119}_{\pm 0.0194}$
2.6500	2.4193	$0.3050^{\pm 0.0296}_{\pm 0.0156}$	$0.3103^{\pm 0.0309}_{\pm 0.0156}$	$0.2301^{\pm 0.0239}_{\pm 0.0114}$	$0.1636^{\pm 0.0172}_{\pm 0.0090}$	$0.1578^{\pm 0.0171}_{\pm 0.0115}$
2.7500	2.4578	$0.3154^{\pm 0.0326}_{\pm 0.0162}$	$0.2764^{\pm 0.0300}_{\pm 0.0142}$	$0.2483^{\pm 0.0282}_{\pm 0.0127}$	$0.2049^{\pm 0.0251}_{\pm 0.0124}$	$0.1663^{\pm 0.0200}_{\pm 0.0119}$
2.8500	2.4957	$0.2298^{\pm 0.0276}_{\pm 0.0118}$	$0.1860^{\pm 0.0244}_{\pm 0.0096}$	$0.2021^{\pm 0.0263}_{\pm 0.0103}$	$0.1920^{\pm 0.0245}_{\pm 0.0103}$	$0.1431^{\pm 0.0201}_{\pm 0.0108}$
2.9500	2.5330	$0.2963^{\pm 0.0381}_{\pm 0.0216}$	$0.2257^{\pm 0.0298}_{\pm 0.0124}$	$0.2635^{\pm 0.0359}_{\pm 0.0137}$	$0.2299^{\pm 0.0317}_{\pm 0.0112}$	$0.1699^{\pm 0.0256}_{\pm 0.0131}$
3.0500	2.5698	$0.2671^{\pm 0.0454}_{\pm 0.0261}$	$0.2547^{\pm 0.0375}_{\pm 0.0244}$	$0.1736^{\pm 0.0295}_{\pm 0.0189}$	$0.1783^{\pm 0.0321}_{\pm 0.0174}$	$0.1900^{\pm 0.0308}_{\pm 0.0172}$
3.1500	2.6061	$0.4051^{\pm 0.0811}_{\pm 0.0441}$	$0.2319^{\pm 0.0463}_{\pm 0.0238}$	$0.2694^{\pm 0.0499}_{\pm 0.0268}$	$0.1827^{\pm 0.0392}_{\pm 0.0189}$	$0.1828^{\pm 0.0392}_{\pm 0.0178}$
3.2500	2.6418	$0.3297^{\pm 0.0666}_{\pm 0.0269}$	$0.2731^{\pm 0.0508}_{\pm 0.0218}$	$0.3078^{\pm 0.0617}_{\pm 0.0289}$	$0.2466^{\pm 0.0506}_{\pm 0.0203}$	$0.1969^{\pm 0.0479}_{\pm 0.0174}$
3.3500	2.6771	$0.2348^{\pm 0.0573}_{\pm 0.0210}$	$0.3011^{\pm 0.0788}_{\pm 0.0257}$	$0.2931^{\pm 0.0590}_{\pm 0.0301}$	$0.1544^{\pm 0.0370}_{\pm 0.0120}$	$0.2338^{\pm 0.0544}_{\pm 0.0281}$
3.4500	2.7119	$0.2516^{\pm 0.0827}_{\pm 0.0260}$	$0.3290^{\pm 0.2141}_{\pm 0.0511}$	$0.2416^{\pm 0.0732}_{\pm 0.0270}$	$0.2867^{\pm 0.0804}_{\pm 0.0304}$	$0.1950^{\pm 0.0496}_{\pm 0.0261}$
3.5500	2.7463	$0.2255^{\pm 0.1258}_{\pm 0.0458}$	$0.1608^{\pm 0.0558}_{\pm 0.0186}$	$0.2188^{\pm 0.0741}_{\pm 0.0222}$	$0.3006^{\pm 0.0880}_{\pm 0.0358}$	$0.1310^{\pm 0.0516}_{\pm 0.0186}$

TABLE VI. $d\sigma/dt$ (μb/GeV^2) vs $|t - t_{\min}|$ (GeV^2) for different photon beam energies. Superscripts are statistical errors and subscripts are systematic errors.

E_γ (GeV)	$\sqrt{s}$ (GeV)	$\lvert t - t_{\min}\rvert$ (GeV^2)				
		0.660	0.700	0.740	0.780	0.820
1.6500	1.9942	$0.0347^{\pm 0.0119}_{\pm 0.0067}$	—	—	—	—
1.7500	2.0407	$0.1480^{\pm 0.0107}_{\pm 0.0285}$	$0.1423^{\pm 0.0114}_{\pm 0.0213}$	$0.1288^{\pm 0.0109}_{\pm 0.0644}$	$0.1195^{\pm 0.0121}_{\pm 0.0438}$	$0.1290^{\pm 0.0189}_{\pm 0.0465}$
1.8500	2.0861	$0.1251^{\pm 0.0083}_{\pm 0.0124}$	$0.1492^{\pm 0.0100}_{\pm 0.0177}$	$0.1371^{\pm 0.0085}_{\pm 0.0092}$	$0.1552^{\pm 0.0117}_{\pm 0.0500}$	$0.1782^{\pm 0.0142}_{\pm 0.0232}$
1.9500	2.1306	$0.1114^{\pm 0.0078}_{\pm 0.0209}$	$0.1108^{\pm 0.0091}_{\pm 0.0114}$	$0.0958^{\pm 0.0072}_{\pm 0.0263}$	$0.0988^{\pm 0.0080}_{\pm 0.0176}$	$0.1141^{\pm 0.0094}_{\pm 0.0083}$
2.0500	2.1742	$0.0844^{\pm 0.0075}_{\pm 0.0064}$	$0.0757^{\pm 0.0075}_{\pm 0.0130}$	$0.0807^{\pm 0.0071}_{\pm 0.0078}$	$0.0687^{\pm 0.0067}_{\pm 0.0226}$	$0.0780^{\pm 0.0083}_{\pm 0.0126}$
2.1500	2.2170	$0.1362^{\pm 0.0114}_{\pm 0.0097}$	$0.1118^{\pm 0.0100}_{\pm 0.0111}$	$0.0924^{\pm 0.0076}_{\pm 0.0289}$	$0.1010^{\pm 0.0102}_{\pm 0.0128}$	$0.0853^{\pm 0.0081}_{\pm 0.0074}$
2.2500	2.2589	$0.1288^{\pm 0.0118}_{\pm 0.0091}$	$0.1255^{\pm 0.0118}_{\pm 0.0084}$	$0.1102^{\pm 0.0091}_{\pm 0.0091}$	$0.0913^{\pm 0.0100}_{\pm 0.0133}$	$0.0864^{\pm 0.0088}_{\pm 0.0253}$
2.3500	2.3001	$0.1301^{\pm 0.0146}_{\pm 0.0099}$	$0.1307^{\pm 0.0116}_{\pm 0.0214}$	$0.1129^{\pm 0.0133}_{\pm 0.0264}$	$0.0826^{\pm 0.0083}_{\pm 0.0081}$	$0.0791^{\pm 0.0100}_{\pm 0.0096}$
2.4500	2.3405	$0.2154^{\pm 0.0153}_{\pm 0.0191}$	$0.1804^{\pm 0.0139}_{\pm 0.0144}$	$0.1833^{\pm 0.0142}_{\pm 0.0170}$	$0.1487^{\pm 0.0126}_{\pm 0.0146}$	$0.1444^{\pm 0.0127}_{\pm 0.0221}$
2.5500	2.3803	$0.1337^{\pm 0.0112}_{\pm 0.0161}$	$0.1137^{\pm 0.0097}_{\pm 0.0134}$	$0.1098^{\pm 0.0096}_{\pm 0.0130}$	$0.0964^{\pm 0.0090}_{\pm 0.0227}$	$0.0921^{\pm 0.0089}_{\pm 0.0123}$
2.6500	2.4193	$0.1501^{\pm 0.0179}_{\pm 0.0104}$	$0.1064^{\pm 0.0140}_{\pm 0.0088}$	$0.1117^{\pm 0.0132}_{\pm 0.0081}$	$0.1043^{\pm 0.0134}_{\pm 0.0089}$	$0.1275^{\pm 0.0160}_{\pm 0.0106}$
2.7500	2.4578	$0.1464^{\pm 0.0183}_{\pm 0.0103}$	$0.1325^{\pm 0.0176}_{\pm 0.0097}$	$0.1176^{\pm 0.0163}_{\pm 0.0095}$	$0.1100^{\pm 0.0170}_{\pm 0.0077}$	$0.0804^{\pm 0.0136}_{\pm 0.0083}$
2.8500	2.4957	$0.1594^{\pm 0.0215}_{\pm 0.0113}$	$0.1415^{\pm 0.0216}_{\pm 0.0106}$	$0.1195^{\pm 0.0194}_{\pm 0.0086}$	$0.0980^{\pm 0.0162}_{\pm 0.0074}$	$0.0795^{\pm 0.0151}_{\pm 0.0086}$
2.9500	2.5330	$0.1597^{\pm 0.0253}_{\pm 0.0113}$	$0.1309^{\pm 0.0228}_{\pm 0.0099}$	$0.1271^{\pm 0.0228}_{\pm 0.0095}$	$0.1057^{\pm 0.0201}_{\pm 0.0078}$	$0.0932^{\pm 0.0184}_{\pm 0.0098}$
3.0500	2.5698	$0.1544^{\pm 0.0268}_{\pm 0.0168}$	$0.1012^{\pm 0.0209}_{\pm 0.0092}$	$0.1441^{\pm 0.0259}_{\pm 0.0125}$	$0.1278^{\pm 0.0284}_{\pm 0.0113}$	$0.1289^{\pm 0.0258}_{\pm 0.0216}$
3.1500	2.6061	$0.1687^{\pm 0.0394}_{\pm 0.0156}$	$0.1299^{\pm 0.0316}_{\pm 0.0121}$	$0.1519^{\pm 0.0330}_{\pm 0.0133}$	$0.1769^{\pm 0.0374}_{\pm 0.0157}$	$0.1095^{\pm 0.0278}_{\pm 0.0178}$
3.2500	2.6418	$0.1808^{\pm 0.0454}_{\pm 0.0171}$	$0.2395^{\pm 0.0493}_{\pm 0.0224}$	$0.1369^{\pm 0.0310}_{\pm 0.0128}$	$0.1210^{\pm 0.0293}_{\pm 0.0106}$	$0.1115^{\pm 0.0280}_{\pm 0.0164}$
3.3500	2.6771	$0.2080^{\pm 0.0544}_{\pm 0.0202}$	$0.1995^{\pm 0.0517}_{\pm 0.0194}$	$0.1535^{\pm 0.0430}_{\pm 0.0134}$	$0.1289^{\pm 0.0320}_{\pm 0.0145}$	$0.1217^{\pm 0.0328}_{\pm 0.0181}$
3.4500	2.7119	$0.1865^{\pm 0.0597}_{\pm 0.0264}$	$0.2104^{\pm 0.0600}_{\pm 0.0281}$	$0.1438^{\pm 0.0474}_{\pm 0.0193}$	$0.1405^{\pm 0.0415}_{\pm 0.0206}$	$0.1433^{\pm 0.0436}_{\pm 0.0323}$
3.5500	2.7463	$0.1309^{\pm 0.0468}_{\pm 0.0194}$	$0.2009^{\pm 0.0670}_{\pm 0.0489}$	$0.1237^{\pm 0.0397}_{\pm 0.0164}$	$0.0870^{\pm 0.0350}_{\pm 0.0119}$	$0.1018^{\pm 0.0368}_{\pm 0.0245}$

TABLE VII. $d\sigma/dt$ (μb/GeV^2) vs $|t - t_{\min}|$ (GeV^2) for different photon beam energies. Superscripts are statistical errors and subscripts are systematic errors.

E_γ (GeV)	$\sqrt{s}$ (GeV)	$\lvert t - t_{\min}\rvert$ (GeV^2)				
		0.860	0.900	0.940	0.980	1.020
1.7500	2.0407	$0.0649^{\pm 0.0067}_{\pm 0.0152}$	$0.0187^{\pm 0.0027}_{\pm 0.0053}$	—	—	—
1.8500	2.0861	$0.1699^{\pm 0.0258}_{\pm 0.0531}$	$0.1681^{\pm 0.0285}_{\pm 0.0307}$	$0.1855^{\pm 0.0391}_{\pm 0.0118}$	$0.1666^{\pm 0.0585}_{\pm 0.0117}$	$0.1670^{\pm 0.0617}_{\pm 0.0118}$
1.9500	2.1306	$0.1294^{\pm 0.0124}_{\pm 0.0099}$	$0.1405^{\pm 0.0133}_{\pm 0.0224}$	$0.1427^{\pm 0.0137}_{\pm 0.0091}$	$0.1591^{\pm 0.0168}_{\pm 0.0112}$	$0.1567^{\pm 0.0177}_{\pm 0.0123}$
2.0500	2.1742	$0.0691^{\pm 0.0065}_{\pm 0.0195}$	$0.0738^{\pm 0.0071}_{\pm 0.0107}$	$0.0800^{\pm 0.0078}_{\pm 0.0208}$	$0.0837^{\pm 0.0083}_{\pm 0.0095}$	$0.0769^{\pm 0.0080}_{\pm 0.0087}$
2.1500	2.2170	$0.0795^{\pm 0.0078}_{\pm 0.0068}$	$0.0808^{\pm 0.0086}_{\pm 0.0126}$	$0.0705^{\pm 0.0075}_{\pm 0.0092}$	$0.0641^{\pm 0.0073}_{\pm 0.0072}$	$0.0620^{\pm 0.0074}_{\pm 0.0071}$
2.2500	2.2589	$0.0775^{\pm 0.0081}_{\pm 0.0174}$	$0.0740^{\pm 0.0083}_{\pm 0.0203}$	$0.0726^{\pm 0.0089}_{\pm 0.0069}$	$0.0718^{\pm 0.0089}_{\pm 0.0210}$	$0.0664^{\pm 0.0099}_{\pm 0.0095}$
2.3500	2.3001	$0.0786^{\pm 0.0092}_{\pm 0.0280}$	$0.0841^{\pm 0.0096}_{\pm 0.0130}$	$0.0698^{\pm 0.0093}_{\pm 0.0325}$	$0.0690^{\pm 0.0096}_{\pm 0.0153}$	$0.0680^{\pm 0.0096}_{\pm 0.0097}$
2.4500	2.3405	$0.1335^{\pm 0.0118}_{\pm 0.0127}$	$0.1178^{\pm 0.0109}_{\pm 0.0289}$	$0.1134^{\pm 0.0112}_{\pm 0.0351}$	$0.0888^{\pm 0.0109}_{\pm 0.0311}$	$0.0678^{\pm 0.0095}_{\pm 0.0108}$
2.5500	2.3803	$0.0799^{\pm 0.0082}_{\pm 0.0131}$	$0.0790^{\pm 0.0083}_{\pm 0.0095}$	$0.0747^{\pm 0.0083}_{\pm 0.0145}$	$0.0698^{\pm 0.0092}_{\pm 0.0174}$	$0.0658^{\pm 0.0094}_{\pm 0.0105}$
2.6500	2.4193	$0.0940^{\pm 0.0129}_{\pm 0.0076}$	$0.0701^{\pm 0.0112}_{\pm 0.0053}$	$0.0798^{\pm 0.0125}_{\pm 0.0060}$	$0.0692^{\pm 0.0115}_{\pm 0.0053}$	$0.0563^{\pm 0.0103}_{\pm 0.0067}$
2.7500	2.4578	$0.1119^{\pm 0.0183}_{\pm 0.0086}$	$0.0832^{\pm 0.0145}_{\pm 0.0067}$	$0.0938^{\pm 0.0165}_{\pm 0.0071}$	$0.0690^{\pm 0.0133}_{\pm 0.0064}$	$0.0770^{\pm 0.0147}_{\pm 0.0091}$
2.8500	2.4957	$0.0815^{\pm 0.0158}_{\pm 0.0086}$	$0.0661^{\pm 0.0140}_{\pm 0.0073}$	$0.0644^{\pm 0.0138}_{\pm 0.0075}$	$0.0733^{\pm 0.0158}_{\pm 0.0087}$	$0.0464^{\pm 0.0112}_{\pm 0.0058}$
2.9500	2.5330	$0.0777^{\pm 0.0168}_{\pm 0.0083}$	$0.0864^{\pm 0.0194}_{\pm 0.0092}$	$0.0635^{\pm 0.0160}_{\pm 0.0069}$	$0.0618^{\pm 0.0145}_{\pm 0.0072}$	$0.0458^{\pm 0.0129}_{\pm 0.0059}$
3.0500	2.5698	$0.0527^{\pm 0.0138}_{\pm 0.0086}$	$0.0705^{\pm 0.0187}_{\pm 0.0117}$	$0.0398^{\pm 0.0121}_{\pm 0.0066}$	$0.0481^{\pm 0.0136}_{\pm 0.0082}$	$0.0687^{\pm 0.0197}_{\pm 0.0134}$
3.1500	2.6061	$0.1142^{\pm 0.0318}_{\pm 0.0187}$	$0.0564^{\pm 0.0188}_{\pm 0.0105}$	$0.0836^{\pm 0.0233}_{\pm 0.0137}$	$0.0509^{\pm 0.0174}_{\pm 0.0083}$	$0.0499^{\pm 0.0172}_{\pm 0.0092}$
3.2500	2.6418	$0.0760^{\pm 0.0202}_{\pm 0.0112}$	$0.0747^{\pm 0.0241}_{\pm 0.0118}$	$0.0848^{\pm 0.0236}_{\pm 0.0125}$	$0.0650^{\pm 0.0205}_{\pm 0.0096}$	$0.0437^{\pm 0.0169}_{\pm 0.0100}$
3.3500	2.6771	$0.0799^{\pm 0.0248}_{\pm 0.0118}$	$0.0807^{\pm 0.0260}_{\pm 0.0143}$	$0.0924^{\pm 0.0287}_{\pm 0.0136}$	$0.0819^{\pm 0.0281}_{\pm 0.0125}$	$0.0598^{\pm 0.0237}_{\pm 0.0137}$
3.4500	2.7119	$0.0831^{\pm 0.0301}_{\pm 0.0184}$	$0.1055^{\pm 0.0371}_{\pm 0.0235}$	$0.0951^{\pm 0.0393}_{\pm 0.0211}$	$0.0852^{\pm 0.0322}_{\pm 0.0194}$	$0.0674^{\pm 0.0298}_{\pm 0.0287}$
3.5500	2.7463	$0.1057^{\pm 0.0391}_{\pm 0.0233}$	$0.0847^{\pm 0.0357}_{\pm 0.0187}$	$0.0577^{\pm 0.0294}_{\pm 0.0127}$	$0.0453^{\pm 0.0224}_{\pm 0.0100}$	$0.0575^{\pm 0.0263}_{\pm 0.0258}$

TABLE VIII. $d\sigma/dt$ (μb/GeV^2) vs $|t - t_{\min}|$ (GeV^2) for different photon beam energies. Superscripts are statistical errors and subscripts are systematic errors.

E_γ (GeV)	$\sqrt{s}$ (GeV)	$\lvert t - t_{\min}\rvert$ (GeV^2)				
		1.060	1.100	1.140	1.180	1.220
1.8500	2.0861	$0.1411^{\pm 0.0481}_{\pm 0.0113}$	$0.0672^{\pm 0.0264}_{\pm 0.0054}$	—	—	—
1.9500	2.1306	$0.1671^{\pm 0.0260}_{\pm 0.0134}$	$0.1558^{\pm 0.0252}_{\pm 0.0138}$	$0.1311^{\pm 0.0295}_{\pm 0.0148}$	$0.1175^{\pm 0.0407}_{\pm 0.0135}$	$0.1222^{\pm 0.0400}_{\pm 0.0231}$
2.0500	2.1742	$0.0818^{\pm 0.0092}_{\pm 0.0110}$	$0.0859^{\pm 0.0099}_{\pm 0.0118}$	$0.0902^{\pm 0.0108}_{\pm 0.0111}$	$0.0933^{\pm 0.0115}_{\pm 0.0116}$	$0.1138^{\pm 0.0153}_{\pm 0.0156}$
2.1500	2.2170	$0.0655^{\pm 0.0080}_{\pm 0.0088}$	$0.0605^{\pm 0.0076}_{\pm 0.0082}$	$0.0606^{\pm 0.0077}_{\pm 0.0075}$	$0.0589^{\pm 0.0078}_{\pm 0.0073}$	$0.0546^{\pm 0.0077}_{\pm 0.0075}$
2.2500	2.2589	$0.0707^{\pm 0.0097}_{\pm 0.0144}$	$0.0627^{\pm 0.0089}_{\pm 0.0130}$	$0.0564^{\pm 0.0082}_{\pm 0.0113}$	$0.0541^{\pm 0.0076}_{\pm 0.0108}$	$0.0546^{\pm 0.0079}_{\pm 0.0099}$
2.3500	2.3001	$0.0587^{\pm 0.0088}_{\pm 0.0120}$	$0.0522^{\pm 0.0087}_{\pm 0.0107}$	$0.0479^{\pm 0.0070}_{\pm 0.0096}$	$0.0415^{\pm 0.0070}_{\pm 0.0083}$	$0.0414^{\pm 0.0073}_{\pm 0.0075}$
2.4500	2.3405	$0.0611^{\pm 0.0086}_{\pm 0.0106}$	$0.0624^{\pm 0.0088}_{\pm 0.0108}$	$0.0598^{\pm 0.0079}_{\pm 0.0105}$	$0.0639^{\pm 0.0082}_{\pm 0.0126}$	$0.0567^{\pm 0.0080}_{\pm 0.0118}$
2.5500	2.3803	$0.0554^{\pm 0.0083}_{\pm 0.0101}$	$0.0521^{\pm 0.0084}_{\pm 0.0096}$	$0.0505^{\pm 0.0079}_{\pm 0.0099}$	$0.0479^{\pm 0.0075}_{\pm 0.0093}$	$0.0410^{\pm 0.0067}_{\pm 0.0085}$
2.6500	2.4193	$0.0675^{\pm 0.0128}_{\pm 0.0080}$	$0.0568^{\pm 0.0117}_{\pm 0.0067}$	$0.0515^{\pm 0.0106}_{\pm 0.0061}$	$0.0597^{\pm 0.0132}_{\pm 0.0070}$	$0.0499^{\pm 0.0125}_{\pm 0.0075}$
2.7500	2.4578	$0.0594^{\pm 0.0123}_{\pm 0.0073}$	$0.0542^{\pm 0.0124}_{\pm 0.0064}$	$0.0528^{\pm 0.0121}_{\pm 0.0063}$	$0.0423^{\pm 0.0120}_{\pm 0.0051}$	$0.0300^{\pm 0.0086}_{\pm 0.0045}$
2.8500	2.4957	$0.0483^{\pm 0.0114}_{\pm 0.0069}$	$0.0398^{\pm 0.0105}_{\pm 0.0051}$	$0.0464^{\pm 0.0134}_{\pm 0.0058}$	$0.0442^{\pm 0.0142}_{\pm 0.0055}$	$0.0587^{\pm 0.0176}_{\pm 0.0093}$
2.9500	2.5330	$0.0570^{\pm 0.0158}_{\pm 0.0072}$	$0.0532^{\pm 0.0150}_{\pm 0.0068}$	$0.0448^{\pm 0.0155}_{\pm 0.0056}$	$0.0463^{\pm 0.0145}_{\pm 0.0059}$	$0.0417^{\pm 0.0165}_{\pm 0.0065}$
3.0500	2.5698	$0.0809^{\pm 0.0244}_{\pm 0.0144}$	$0.0495^{\pm 0.0150}_{\pm 0.0089}$	$0.0642^{\pm 0.0207}_{\pm 0.0119}$	$0.0500^{\pm 0.0190}_{\pm 0.0089}$	$0.0741^{\pm 0.0280}_{\pm 0.0239}$
3.1500	2.6061	$0.0585^{\pm 0.0209}_{\pm 0.0106}$	$0.0608^{\pm 0.0217}_{\pm 0.0116}$	$0.0644^{\pm 0.0243}_{\pm 0.0116}$	$0.0603^{\pm 0.0254}_{\pm 0.0109}$	$0.0600^{\pm 0.0277}_{\pm 0.0202}$
3.2500	2.6418	$0.0623^{\pm 0.0232}_{\pm 0.0143}$	$0.0560^{\pm 0.0218}_{\pm 0.0130}$	$0.0430^{\pm 0.0172}_{\pm 0.0099}$	$0.0518^{\pm 0.0235}_{\pm 0.0120}$	$0.0506^{\pm 0.0237}_{\pm 0.0274}$
3.3500	2.6771	$0.0457^{\pm 0.0208}_{\pm 0.0105}$	$0.0635^{\pm 0.0244}_{\pm 0.0148}$	$0.0462^{\pm 0.0224}_{\pm 0.0106}$	$0.0285^{\pm 0.0138}_{\pm 0.0066}$	$0.0609^{\pm 0.0333}_{\pm 0.0332}$
3.4500	2.7119	$0.0856^{\pm 0.0325}_{\pm 0.0366}$	$0.0538^{\pm 0.0215}_{\pm 0.0228}$	$0.0362^{\pm 0.0179}_{\pm 0.0156}$	$0.0522^{\pm 0.0263}_{\pm 0.0223}$	$0.0325^{\pm 0.0190}_{\pm 0.0220}$
3.5500	2.7463	$0.0439^{\pm 0.0248}_{\pm 0.0188}$	$0.0473^{\pm 0.0246}_{\pm 0.0202}$	$0.0266^{\pm 0.0174}_{\pm 0.0113}$	$0.0564^{\pm 0.0252}_{\pm 0.0239}$	$0.0453^{\pm 0.0326}_{\pm 0.0307}$

TABLE IX. $d\sigma/dt$ (μb/GeV^2) vs $|t - t_{\min}|$ (GeV^2) for different photon beam energies. Superscripts are statistical errors and subscripts are systematic errors.

E_γ (GeV)	$\sqrt{s}$ (GeV)	$\lvert t - t_{\min}\rvert$ (GeV^2)				
		1.260	1.300	1.340	1.380	1.420
1.9500	2.1306	$0.1042^{\pm 0.0378}_{\pm 0.0199}$	$0.0473^{\pm 0.0181}_{\pm 0.0109}$	$0.0241^{\pm 0.0049}_{\pm 0.0056}$	$0.0279^{\pm 0.0061}_{\pm 0.0206}$	$0.0074^{\pm 0.0026}_{\pm 0.0054}$
2.0500	2.1742	$0.0959^{\pm 0.0191}_{\pm 0.0131}$	$0.1046^{\pm 0.0242}_{\pm 0.0140}$	$0.0890^{\pm 0.0280}_{\pm 0.0120}$	$0.1034^{\pm 0.0351}_{\pm 0.0150}$	$0.0860^{\pm 0.0310}_{\pm 0.0125}$
2.1500	2.2170	$0.0642^{\pm 0.0092}_{\pm 0.0088}$	$0.0669^{\pm 0.0104}_{\pm 0.0090}$	$0.0680^{\pm 0.0105}_{\pm 0.0091}$	$0.0787^{\pm 0.0133}_{\pm 0.0114}$	n$0.0855^{\pm 0.0182}_{\pm 0.0125}$
2.2500	2.2589	$0.0519^{\pm 0.0078}_{\pm 0.0094}$	$0.0596^{\pm 0.0085}_{\pm 0.0086}$	$0.0497^{\pm 0.0077}_{\pm 0.0073}$	$0.0526^{\pm 0.0084}_{\pm 0.0088}$	$0.0663^{\pm 0.0114}_{\pm 0.0111}$
2.3500	2.3001	$0.0508^{\pm 0.0087}_{\pm 0.0093}$	$0.0458^{\pm 0.0081}_{\pm 0.0066}$	$0.0413^{\pm 0.0075}_{\pm 0.0062}$	$0.0407^{\pm 0.0076}_{\pm 0.0068}$	$0.0399^{\pm 0.0077}_{\pm 0.0067}$
2.4500	2.3405	$0.0535^{\pm 0.0074}_{\pm 0.0112}$	$0.0511^{\pm 0.0078}_{\pm 0.0134}$	$0.0443^{\pm 0.0069}_{\pm 0.0117}$	$0.0464^{\pm 0.0071}_{\pm 0.0204}$	$0.0431^{\pm 0.0071}_{\pm 0.0190}$
2.5500	2.3803	$0.0419^{\pm 0.0072}_{\pm 0.0088}$	$0.0397^{\pm 0.0068}_{\pm 0.0104}$	$0.0257^{\pm 0.0049}_{\pm 0.0067}$	$0.0234^{\pm 0.0044}_{\pm 0.0103}$	$0.0190^{\pm 0.0040}_{\pm 0.0083}$
2.6500	2.4193	$0.0355^{\pm 0.0093}_{\pm 0.0053}$	$0.0357^{\pm 0.0099}_{\pm 0.0056}$	$0.0308^{\pm 0.0099}_{\pm 0.0046}$	$0.0318^{\pm 0.0104}_{\pm 0.0048}$	$0.0225^{\pm 0.0081}_{\pm 0.0083}$
2.7500	2.4578	$0.0365^{\pm 0.0114}_{\pm 0.0055}$	$0.0432^{\pm 0.0144}_{\pm 0.0065}$	$0.0337^{\pm 0.0126}_{\pm 0.0050}$	$0.0386^{\pm 0.0142}_{\pm 0.0061}$	$0.0522^{\pm 0.0196}_{\pm 0.0194}$
2.8500	2.4957	$0.0527^{\pm 0.0175}_{\pm 0.0084}$	$0.0576^{\pm 0.0196}_{\pm 0.0090}$	$0.0351^{\pm 0.0150}_{\pm 0.0055}$	$0.0452^{\pm 0.0182}_{\pm 0.0071}$	$0.0530^{\pm 0.0243}_{\pm 0.0097}$
2.9500	2.5330	$0.0449^{\pm 0.0163}_{\pm 0.0075}$	$0.0461^{\pm 0.0195}_{\pm 0.0072}$	$0.0283^{\pm 0.0110}_{\pm 0.0044}$	$0.0529^{\pm 0.0265}_{\pm 0.0084}$	$0.0453^{\pm 0.0225}_{\pm 0.0083}$
3.0500	2.5698	$0.0614^{\pm 0.0232}_{\pm 0.0197}$	$0.0704^{\pm 0.0289}_{\pm 0.0227}$	$0.0626^{\pm 0.0296}_{\pm 0.0201}$	$0.0417^{\pm 0.0192}_{\pm 0.0134}$	$0.0362^{\pm 0.0178}_{\pm 0.0128}$
3.1500	2.6061	$0.0482^{\pm 0.0225}_{\pm 0.0155}$	$0.0667^{\pm 0.0336}_{\pm 0.0214}$	$0.0594^{\pm 0.0280}_{\pm 0.0192}$	$0.0431^{\pm 0.0231}_{\pm 0.0139}$	$0.0606^{\pm 0.0292}_{\pm 0.0215}$
3.2500	2.6418	$0.0324^{\pm 0.0150}_{\pm 0.0177}$	$0.0345^{\pm 0.0181}_{\pm 0.0188}$	$0.0388^{\pm 0.0213}_{\pm 0.0212}$	$0.0305^{\pm 0.0175}_{\pm 0.0165}$	$0.0314^{\pm 0.0170}_{\pm 0.0190}$
3.3500	2.6771	$0.0491^{\pm 0.0255}_{\pm 0.0272}$	$0.0499^{\pm 0.0295}_{\pm 0.0272}$	$0.0565^{\pm 0.0301}_{\pm 0.0306}$	$0.0344^{\pm 0.0212}_{\pm 0.0187}$	$0.0251^{\pm 0.0180}_{\pm 0.0153}$
3.4500	2.7119	$0.0194^{\pm 0.0110}_{\pm 0.0133}$	$0.0264^{\pm 0.0165}_{\pm 0.0179}$	$0.0389^{\pm 0.0212}_{\pm 0.0265}$	$0.0111^{\pm 0.0087}_{\pm 0.0075}$	$0.0304^{\pm 0.0239}_{\pm 0.0196}$
3.5500	2.7463	$0.0254^{\pm 0.0177}_{\pm 0.0172}$	$0.0136^{\pm 0.0123}_{\pm 0.0092}$	$0.0300^{\pm 0.0247}_{\pm 0.0203}$	$0.0152^{\pm 0.0167}_{\pm 0.0103}$	$0.0320^{\pm 0.0299}_{\pm 0.0224}$

TABLE X. $d\sigma/dt$ (μb/GeV^2) vs $|t - t_{\min}|$ (GeV^2) for different photon beam energies. Superscripts are statistical errors and subscripts are systematic errors.

E_γ (GeV)	$\sqrt{s}$ (GeV)	$\lvert t - t_{\min}\rvert$ (GeV^2)				
		1.460	1.500	1.540	1.580	1.620
2.0500	2.1742	$0.0519^{\pm 0.0204}_{\pm 0.0060}$	$0.0232^{\pm 0.0110}_{\pm 0.0027}$	$0.0157^{\pm 0.0085}_{\pm 0.0027}$	—	—
2.1500	2.2170	$0.0754^{\pm 0.0214}_{\pm 0.0088}$	$0.0771^{\pm 0.0272}_{\pm 0.0090}$	$0.0801^{\pm 0.0285}_{\pm 0.0139}$	$0.0647^{\pm 0.0293}_{\pm 0.0112}$	$0.0557^{\pm 0.0249}_{\pm 0.0180}$
2.2500	2.2589	$0.0641^{\pm 0.0111}_{\pm 0.0129}$	$0.0545^{\pm 0.0101}_{\pm 0.0110}$	$0.0684^{\pm 0.0143}_{\pm 0.0149}$	$0.0979^{\pm 0.0211}_{\pm 0.0206}$	$0.0796^{\pm 0.0227}_{\pm 0.0174}$
2.3500	2.3001	$0.0349^{\pm 0.0069}_{\pm 0.0070}$	$0.0360^{\pm 0.0075}_{\pm 0.0073}$	$0.0359^{\pm 0.0076}_{\pm 0.0078}$	$0.0375^{\pm 0.0103}_{\pm 0.0083}$	$0.0312^{\pm 0.0100}_{\pm 0.0068}$
2.4500	2.3405	$0.0412^{\pm 0.0072}_{\pm 0.0156}$	$0.0418^{\pm 0.0067}_{\pm 0.0158}$	$0.0412^{\pm 0.0068}_{\pm 0.0131}$	$0.0440^{\pm 0.0066}_{\pm 0.0139}$	$0.0351^{\pm 0.0061}_{\pm 0.0144}$
2.5500	2.3803	$0.0269^{\pm 0.0054}_{\pm 0.0102}$	$0.0308^{\pm 0.0062}_{\pm 0.0117}$	$0.0329^{\pm 0.0065}_{\pm 0.0105}$	$0.0461^{\pm 0.0090}_{\pm 0.0147}$	$0.0381^{\pm 0.0078}_{\pm 0.0157}$
2.6500	2.4193	$0.0345^{\pm 0.0130}_{\pm 0.0128}$	$0.0444^{\pm 0.0177}_{\pm 0.0165}$	$0.0350^{\pm 0.0155}_{\pm 0.0130}$	$0.0313^{\pm 0.0149}_{\pm 0.0116}$	$0.0361^{\pm 0.0171}_{\pm 0.0116}$
2.7500	2.4578	$0.0311^{\pm 0.0137}_{\pm 0.0115}$	$0.0326^{\pm 0.0143}_{\pm 0.0122}$	$0.0335^{\pm 0.0169}_{\pm 0.0129}$	$0.0269^{\pm 0.0130}_{\pm 0.0102}$	$0.0242^{\pm 0.0147}_{\pm 0.0078}$
2.8500	2.4957	$0.0501^{\pm 0.0235}_{\pm 0.0092}$	$0.0500^{\pm 0.0257}_{\pm 0.0091}$	$0.0381^{\pm 0.0220}_{\pm 0.0070}$	$0.0449^{\pm 0.0296}_{\pm 0.0082}$	—
2.9500	2.5330	$0.0402^{\pm 0.0222}_{\pm 0.0073}$	$0.0413^{\pm 0.0236}_{\pm 0.0076}$	$0.0309^{\pm 0.0193}_{\pm 0.0056}$	$0.0464^{\pm 0.0344}_{\pm 0.0089}$	—
3.0500	2.5698	$0.0352^{\pm 0.0183}_{\pm 0.0124}$	$0.0297^{\pm 0.0205}_{\pm 0.0105}$	$0.0450^{\pm 0.0319}_{\pm 0.0159}$	$0.0431^{\pm 0.0354}_{\pm 0.0152}$	—
3.1500	2.6061	$0.0706^{\pm 0.0392}_{\pm 0.0250}$	$0.0269^{\pm 0.0201}_{\pm 0.0095}$	$0.0505^{\pm 0.0390}_{\pm 0.0179}$	$0.0321^{\pm 0.0252}_{\pm 0.0113}$	—
3.2500	2.6418	$0.0357^{\pm 0.0226}_{\pm 0.0217}$	$0.0270^{\pm 0.0198}_{\pm 0.0164}$	$0.0342^{\pm 0.0235}_{\pm 0.0207}$	$0.0092^{\pm 0.0082}_{\pm 0.0055}$	—
3.3500	2.6771	$0.0307^{\pm 0.0231}_{\pm 0.0186}$	$0.0319^{\pm 0.0251}_{\pm 0.0193}$	$0.0287^{\pm 0.0218}_{\pm 0.0173}$	$0.0241^{\pm 0.0195}_{\pm 0.0146}$	—
3.4500	2.7119	$0.0416^{\pm 0.0339}_{\pm 0.0291}$	$0.0403^{\pm 0.0348}_{\pm 0.0323}$	$0.0313^{\pm 0.0311}_{\pm 0.0219}$	$0.0326^{\pm 0.0293}_{\pm 0.0260}$	—
3.5500	2.7463	$0.0106^{\pm 0.0108}_{\pm 0.0085}$	$0.0178^{\pm 0.0175}_{\pm 0.0142}$	$0.0175^{\pm 0.0184}_{\pm 0.0140}$	$0.0325^{\pm 0.0324}_{\pm 0.0234}$	—

TABLE XI. $d\sigma/dt$ (μb/GeV^2) vs $|t - t_{\min}|$ (GeV^2) for different photon beam energies. Superscripts are statistical errors and subscripts are systematic errors.

E_γ (GeV)	$\sqrt{s}$ (GeV)	$\lvert t - t_{\min}\rvert$ (GeV^2)				
		1.660	1.700	1.740	1.780	1.820
2.1500	2.2170	$0.0382^{\pm 0.0163}_{\pm 0.0124}$	$0.0259^{\pm 0.0140}_{\pm 0.0158}$	$0.0257^{\pm 0.0053}_{\pm 0.0159}$	$0.0196^{\pm 0.0047}_{\pm 0.0121}$	—
2.2500	2.2589	$0.0923^{\pm 0.0323}_{\pm 0.0202}$	$0.0850^{\pm 0.0356}_{\pm 0.0216}$	$0.0835^{\pm 0.0449}_{\pm 0.0213}$	$0.0705^{\pm 0.0400}_{\pm 0.0130}$	—
2.3500	2.3001	$0.0433^{\pm 0.0108}_{\pm 0.0096}$	$0.0562^{\pm 0.0145}_{\pm 0.0143}$	$0.0677^{\pm 0.0192}_{\pm 0.0172}$	$0.0704^{\pm 0.0198}_{\pm 0.0130}$	—
2.4500	2.3405	$0.0401^{\pm 0.0074}_{\pm 0.0165}$	$0.0361^{\pm 0.0069}_{\pm 0.0205}$	—	—	—
2.5500	2.3803	$0.0347^{\pm 0.0076}_{\pm 0.0143}$	$0.0303^{\pm 0.0069}_{\pm 0.0178}$	—	—	—
2.6500	2.4193	$0.0306^{\pm 0.0180}_{\pm 0.0098}$	$0.0260^{\pm 0.0179}_{\pm 0.0083}$	—	—	—
2.7500	2.4578	$0.0212^{\pm 0.0133}_{\pm 0.0068}$	$0.0219^{\pm 0.0174}_{\pm 0.0070}$	—	—	—

APPENDIX B

The following data tables include measured differential cross section $d\sigma/dt$ for different photon beam energy and $\cos\theta_{\text{c.m.}}$ values.

TABLE XII. $d\sigma/dt$ (μb/GeV^2) vs $\cos\theta_{\text{c.m.}}$ (GeV) for different photon beam energies. Superscripts are statistical errors and subscripts are systematic errors.

$\cos\theta_{\text{c.m.}}$	E_γ (GeV)				
	1.650	1.750	1.850	1.950	2.050
−0.4000	—	$0.2215^{\pm0.0111}_{\pm0.0240}$	$0.1334^{\pm0.0095}_{\pm0.0242}$	$0.1212^{\pm0.0091}_{\pm0.0241}$	$0.0642^{\pm0.0053}_{\pm0.0145}$
−0.3000	—	$0.1687^{\pm0.0073}_{\pm0.0174}$	$0.1368^{\pm0.0074}_{\pm0.0217}$	$0.1136^{\pm0.0075}_{\pm0.0230}$	$0.0546^{\pm0.0056}_{\pm0.0123}$
−0.2000	$0.1506^{\pm0.0084}_{\pm0.0242}$	$0.2013^{\pm0.0080}_{\pm0.0178}$	$0.1280^{\pm0.0062}_{\pm0.0175}$	$0.1126^{\pm0.0074}_{\pm0.0174}$	$0.0528^{\pm0.0034}_{\pm0.0114}$
−0.1000	$0.1902^{\pm0.0105}_{\pm0.0251}$	$0.1941^{\pm0.0073}_{\pm0.0178}$	$0.1361^{\pm0.0062}_{\pm0.0119}$	$0.1021^{\pm0.0056}_{\pm0.0191}$	$0.0780^{\pm0.0047}_{\pm0.0155}$
0.0000	$0.2433^{\pm0.0122}_{\pm0.0275}$	$0.1979^{\pm0.0073}_{\pm0.0183}$	$0.1330^{\pm0.0058}_{\pm0.0131}$	$0.0990^{\pm0.0053}_{\pm0.0081}$	$0.0894^{\pm0.0054}_{\pm0.0121}$
0.1000	$0.2102^{\pm0.0103}_{\pm0.0325}$	$0.2384^{\pm0.0077}_{\pm0.0133}$	$0.1504^{\pm0.0058}_{\pm0.0095}$	$0.1112^{\pm0.0051}_{\pm0.0072}$	$0.0830^{\pm0.0046}_{\pm0.0106}$
0.2000	$0.2396^{\pm0.0114}_{\pm0.0208}$	$0.2511^{\pm0.0079}_{\pm0.0146}$	$0.1522^{\pm0.0057}_{\pm0.0083}$	$0.1312^{\pm0.0057}_{\pm0.0083}$	$0.1105^{\pm0.0053}_{\pm0.0143}$
0.3000	$0.2862^{\pm0.0126}_{\pm0.0338}$	$0.2746^{\pm0.0081}_{\pm0.0173}$	$0.1805^{\pm0.0062}_{\pm0.0148}$	$0.1453^{\pm0.0059}_{\pm0.0082}$	$0.1685^{\pm0.0071}_{\pm0.0177}$
0.4000	$0.2923^{\pm0.0125}_{\pm0.0251}$	$0.2851^{\pm0.0083}_{\pm0.0132}$	$0.2402^{\pm0.0075}_{\pm0.0168}$	$0.2185^{\pm0.0080}_{\pm0.0100}$	$0.1962^{\pm0.0076}_{\pm0.0112}$
0.5000	$0.3202^{\pm0.0134}_{\pm0.0176}$	$0.3126^{\pm0.0087}_{\pm0.0140}$	$0.2850^{\pm0.0086}_{\pm0.0123}$	$0.2548^{\pm0.0085}_{\pm0.0155}$	$0.2576^{\pm0.0090}_{\pm0.0108}$
0.6000	$0.3226^{\pm0.0129}_{\pm0.0258}$	$0.3546^{\pm0.0097}_{\pm0.0184}$	$0.3613^{\pm0.0104}_{\pm0.0257}$	$0.3270^{\pm0.0100}_{\pm0.0263}$	$0.3118^{\pm0.0101}_{\pm0.0135}$
0.7000	$0.3065^{\pm0.0122}_{\pm0.0245}$	$0.3789^{\pm0.0102}_{\pm0.0268}$	$0.4184^{\pm0.0111}_{\pm0.0240}$	$0.4554^{\pm0.0130}_{\pm0.0144}$	$0.4072^{\pm0.0125}_{\pm0.0224}$
0.8000	$0.4063^{\pm0.0169}_{\pm0.0298}$	$0.4961^{\pm0.0134}_{\pm0.0244}$	$0.5745^{\pm0.0143}_{\pm0.0371}$	$0.5593^{\pm0.0149}_{\pm0.0258}$	$0.5167^{\pm0.0277}_{\pm0.0192}$
0.9000	—	$0.5173^{\pm0.0152}_{\pm0.0311}$	$0.8667^{\pm0.0231}_{\pm0.0337}$	$0.7979^{\pm0.0229}_{\pm0.0406}$	$0.7180^{\pm0.0248}_{\pm0.0474}$

TABLE XIII. $d\sigma/dt$ (μb/GeV^2) vs $\cos\theta_{\text{c.m.}}$ (GeV) for different photon beam energies. Superscripts are statistical errors and subscripts are systematic errors.

$\cos\theta_{\text{c.m.}}$	E_γ (GeV)				
	2.150	2.250	2.350	2.450	2.550
−0.4000	$0.0594^{\pm0.0061}_{\pm0.0116}$	$0.0538^{\pm0.0072}_{\pm0.0101}$	$0.0386^{\pm0.0069}_{\pm0.0058}$	$0.0143^{\pm0.0021}_{\pm0.0059}$	$0.0143^{\pm0.0024}_{\pm0.0062}$
−0.3000	$0.0408^{\pm0.0039}_{\pm0.0076}$	$0.0423^{\pm0.0045}_{\pm0.0077}$	$0.0305^{\pm0.0042}_{\pm0.0053}$	$0.0125^{\pm0.0017}_{\pm0.0047}$	$0.0112^{\pm0.0016}_{\pm0.0049}$
−0.2000	$0.0418^{\pm0.0035}_{\pm0.0081}$	$0.0418^{\pm0.0042}_{\pm0.0076}$	$0.0320^{\pm0.0041}_{\pm0.0054}$	$0.0210^{\pm0.0027}_{\pm0.0051}$	$0.0201^{\pm0.0026}_{\pm0.0057}$
−0.1000	$0.0397^{\pm0.0033}_{\pm0.0076}$	$0.0364^{\pm0.0035}_{\pm0.0077}$	$0.0335^{\pm0.0039}_{\pm0.0067}$	$0.0340^{\pm0.0033}_{\pm0.0060}$	$0.0310^{\pm0.0036}_{\pm0.0054}$
0.0000	$0.0719^{\pm0.0053}_{\pm0.0111}$	$0.0539^{\pm0.0048}_{\pm0.0108}$	$0.0304^{\pm0.0033}_{\pm0.0054}$	$0.0329^{\pm0.0030}_{\pm0.0078}$	$0.0242^{\pm0.0028}_{\pm0.0057}$
0.1000	$0.0841^{\pm0.0056}_{\pm0.0103}$	$0.0784^{\pm0.0078}_{\pm0.0121}$	$0.0477^{\pm0.0045}_{\pm0.0081}$	$0.0379^{\pm0.0032}_{\pm0.0069}$	$0.0397^{\pm0.0039}_{\pm0.0067}$
0.2000	$0.1045^{\pm0.0062}_{\pm0.0123}$	$0.0895^{\pm0.0062}_{\pm0.0113}$	$0.0805^{\pm0.0071}_{\pm0.0144}$	$0.0501^{\pm0.0041}_{\pm0.0081}$	$0.0532^{\pm0.0048}_{\pm0.0077}$
0.3000	$0.1259^{\pm0.0067}_{\pm0.0078}$	$0.1141^{\pm0.0062}_{\pm0.0111}$	$0.0982^{\pm0.0068}_{\pm0.0077}$	$0.0900^{\pm0.0052}_{\pm0.0113}$	$0.0745^{\pm0.0063}_{\pm0.0102}$
0.4000	$0.1539^{\pm0.0073}_{\pm0.0096}$	$0.1409^{\pm0.0072}_{\pm0.0086}$	$0.1177^{\pm0.0067}_{\pm0.0096}$	$0.1220^{\pm0.0063}_{\pm0.0101}$	$0.1116^{\pm0.0088}_{\pm0.0120}$
0.5000	$0.2007^{\pm0.0084}_{\pm0.0128}$	$0.2113^{\pm0.0088}_{\pm0.0121}$	$0.1526^{\pm0.0070}_{\pm0.0074}$	$0.1694^{\pm0.0075}_{\pm0.0105}$	$0.1486^{\pm0.0106}_{\pm0.0100}$
0.6000	$0.2713^{\pm0.0093}_{\pm0.0102}$	$0.2044^{\pm0.0080}_{\pm0.0099}$	$0.2369^{\pm0.0104}_{\pm0.0153}$	$0.2206^{\pm0.0099}_{\pm0.0154}$	$0.2083^{\pm0.0150}_{\pm0.0150}$
0.7000	$0.3208^{\pm0.0110}_{\pm0.0141}$	$0.3082^{\pm0.0115}_{\pm0.0166}$	$0.3011^{\pm0.0112}_{\pm0.0134}$	$0.2787^{\pm0.0117}_{\pm0.0128}$	$0.2656^{\pm0.0189}_{\pm0.0205}$
0.8000	$0.4965^{\pm0.0165}_{\pm0.0215}$	$0.4433^{\pm0.0153}_{\pm0.0260}$	$0.4442^{\pm0.0183}_{\pm0.0233}$	$0.3782^{\pm0.0150}_{\pm0.0160}$	$0.3676^{\pm0.0267}_{\pm0.0257}$
0.9000	$0.7900^{\pm0.0323}_{\pm0.0435}$	$0.6411^{\pm0.0261}_{\pm0.0266}$	$0.5566^{\pm0.0279}_{\pm0.0306}$	$0.4633^{\pm0.0225}_{\pm0.0238}$	$0.5053^{\pm0.0494}_{\pm0.0244}$

TABLE XIV. $d\sigma/dt$ (μb/GeV^2) vs $\cos\theta_{\text{c.m.}}$ for different photon beam energies. Superscripts are statistical errors and subscripts are systematic errors.

$\cos\theta_{\text{c.m.}}$	E_γ (GeV)				
	2.650	2.750	2.850	2.950	3.050
−0.4000	$0.0079^{\pm0.0057}_{\pm0.0056}$	$0.0067^{\pm0.0013}_{\pm0.0049}$	—	—	—
−0.3000	$0.0135^{\pm0.0021}_{\pm0.0097}$	$0.0136^{\pm0.0064}_{\pm0.0093}$	—	—	—
−0.2000	$0.0153^{\pm0.0021}_{\pm0.0107}$	$0.0128^{\pm0.0022}_{\pm0.0089}$	—	—	—
−0.1000	$0.0129^{\pm0.0018}_{\pm0.0052}$	$0.0095^{\pm0.0018}_{\pm0.0040}$	$0.0219^{\pm0.0027}_{\pm0.0139}$	$0.0137^{\pm0.0023}_{\pm0.0076}$	$0.0066^{\pm0.0034}_{\pm0.0057}$
0.0000	$0.0184^{\pm0.0022}_{\pm0.0081}$	$0.0116^{\pm0.0017}_{\pm0.0048}$	$0.0225^{\pm0.0032}_{\pm0.0082}$	$0.0157^{\pm0.0027}_{\pm0.0058}$	$0.0074^{\pm0.0017}_{\pm0.0055}$
0.1000	$0.0233^{\pm0.0027}_{\pm0.0056}$	$0.0241^{\pm0.0028}_{\pm0.0061}$	$0.0312^{\pm0.0036}_{\pm0.0082}$	$0.0243^{\pm0.0035}_{\pm0.0069}$	$0.0117^{\pm0.0022}_{\pm0.0075}$
0.2000	$0.0394^{\pm0.0039}_{\pm0.0053}$	$0.0280^{\pm0.0035}_{\pm0.0037}$	$0.0328^{\pm0.0038}_{\pm0.0069}$	$0.0254^{\pm0.0034}_{\pm0.0064}$	$0.0138^{\pm0.0024}_{\pm0.0058}$
0.3000	$0.0494^{\pm0.0044}_{\pm0.0060}$	$0.0382^{\pm0.0043}_{\pm0.0046}$	$0.0351^{\pm0.0041}_{\pm0.0051}$	$0.0287^{\pm0.0039}_{\pm0.0040}$	$0.0474^{\pm0.0061}_{\pm0.0086}$
0.4000	$0.0633^{\pm0.0054}_{\pm0.0058}$	$0.0659^{\pm0.0062}_{\pm0.0061}$	$0.0468^{\pm0.0050}_{\pm0.0058}$	$0.0422^{\pm0.0052}_{\pm0.0053}$	$0.0444^{\pm0.0057}_{\pm0.0093}$
0.5000	$0.0928^{\pm0.0070}_{\pm0.0079}$	$0.0833^{\pm0.0076}_{\pm0.0071}$	$0.0687^{\pm0.0070}_{\pm0.0068}$	$0.0660^{\pm0.0077}_{\pm0.0063}$	$0.0422^{\pm0.0058}_{\pm0.0082}$
0.6000	$0.1327^{\pm0.0100}_{\pm0.0083}$	$0.1222^{\pm0.0102}_{\pm0.0077}$	$0.1313^{\pm0.0117}_{\pm0.0096}$	$0.1159^{\pm0.0116}_{\pm0.0082}$	$0.1083^{\pm0.0120}_{\pm0.0127}$
0.7000	$0.2510^{\pm0.0195}_{\pm0.0129}$	$0.2239^{\pm0.0181}_{\pm0.0123}$	$0.1846^{\pm0.0160}_{\pm0.0095}$	$0.2089^{\pm0.0192}_{\pm0.0143}$	$0.1637^{\pm0.0178}_{\pm0.0130}$
0.8000	$0.3070^{\pm0.0254}_{\pm0.0140}$	$0.3217^{\pm0.0276}_{\pm0.0153}$	$0.3215^{\pm0.0312}_{\pm0.0158}$	$0.2974^{\pm0.0331}_{\pm0.0148}$	$0.3350^{\pm0.0395}_{\pm0.0207}$
0.9000	$0.5552^{\pm0.0634}_{\pm0.0290}$	$0.5942^{\pm0.0795}_{\pm0.0322}$	$0.6169^{\pm0.0850}_{\pm0.0358}$	$0.6322^{\pm0.1151}_{\pm0.0426}$	$0.6110^{\pm0.1237}_{\pm0.0538}$

TABLE XV. $d\sigma/dt$ (μb/GeV^2) vs $\cos\theta_{\text{c.m.}}$ for different photon beam energies. Superscripts are statistical errors and subscripts are systematic errors.

$\cos\theta_{\text{c.m.}}$	E_γ (GeV)				
	3.150	3.250	3.350	3.450	3.550
−0.1000	$0.0054^{\pm0.0017}_{\pm0.0043}$	$0.0039^{\pm0.0012}_{\pm0.0032}$	$0.0041^{\pm0.0017}_{\pm0.0034}$	$0.0042^{\pm0.0018}_{\pm0.0038}$	$0.0022^{\pm0.0012}_{\pm0.0020}$
0.0000	$0.0069^{\pm0.0023}_{\pm0.0048}$	$0.0026^{\pm0.0017}_{\pm0.0023}$	$0.0028^{\pm0.0010}_{\pm0.0022}$	$0.0024^{\pm0.0011}_{\pm0.0023}$	$0.0024^{\pm0.0015}_{\pm0.0022}$
0.1000	$0.0094^{\pm0.0024}_{\pm0.0057}$	$0.0061^{\pm0.0015}_{\pm0.0038}$	$0.0075^{\pm0.0020}_{\pm0.0043}$	$0.0050^{\pm0.0024}_{\pm0.0043}$	$0.0041^{\pm0.0035}_{\pm0.0036}$
0.2000	$0.0174^{\pm0.0038}_{\pm0.0084}$	$0.0086^{\pm0.0019}_{\pm0.0044}$	$0.0072^{\pm0.0019}_{\pm0.0035}$	$0.0073^{\pm0.0022}_{\pm0.0055}$	$0.0055^{\pm0.0026}_{\pm0.0044}$
0.3000	$0.0387^{\pm0.0060}_{\pm0.0080}$	$0.0179^{\pm0.0033}_{\pm0.0061}$	$0.0130^{\pm0.0027}_{\pm0.0055}$	$0.0252^{\pm0.0046}_{\pm0.0105}$	$0.0131^{\pm0.0037}_{\pm0.0081}$
0.4000	$0.0414^{\pm0.0069}_{\pm0.0087}$	$0.0301^{\pm0.0048}_{\pm0.0073}$	$0.0294^{\pm0.0049}_{\pm0.0107}$	$0.0140^{\pm0.0031}_{\pm0.0084}$	$0.0124^{\pm0.0034}_{\pm0.0064}$
0.5000	$0.0463^{\pm0.0074}_{\pm0.0090}$	$0.0448^{\pm0.0067}_{\pm0.0103}$	$0.0441^{\pm0.0076}_{\pm0.0111}$	$0.0394^{\pm0.0069}_{\pm0.0108}$	$0.0318^{\pm0.0072}_{\pm0.0118}$
0.6000	$0.1145^{\pm0.0152}_{\pm0.0152}$	$0.0868^{\pm0.0117}_{\pm0.0111}$	$0.0768^{\pm0.0111}_{\pm0.0098}$	$0.0823^{\pm0.0133}_{\pm0.0115}$	$0.0538^{\pm0.0111}_{\pm0.0099}$
0.7000	$0.1708^{\pm0.0225}_{\pm0.0125}$	$0.2053^{\pm0.0266}_{\pm0.0160}$	$0.1952^{\pm0.0276}_{\pm0.0172}$	$0.1762^{\pm0.0270}_{\pm0.0188}$	$0.1219^{\pm0.0219}_{\pm0.0132}$
0.8000	$0.3292^{\pm0.0444}_{\pm0.0200}$	$0.3166^{\pm0.0462}_{\pm0.0228}$	$0.2496^{\pm0.0429}_{\pm0.0187}$	$0.2298^{\pm0.0481}_{\pm0.0233}$	$0.1788^{\pm0.0395}_{\pm0.0184}$
0.9000	$0.6351^{\pm0.1402}_{\pm0.0577}$	$0.5407^{\pm0.1414}_{\pm0.0545}$	$0.5969^{\pm0.2243}_{\pm0.0611}$	$0.5216^{\pm0.1725}_{\pm0.0945}$	$0.3243^{\pm0.1841}_{\pm0.0572}$

APPENDIX C

The following data table includes measured cross section $d\sigma/dt$ at $|t - t_{\min}|$ and the B slope of the cross section t dependence for different photon beam energy values.

TABLE XVI. $d\sigma/dt(|t| = |t|_{\min})$ (μb/GeV^2) and B (GeV^{-2}) vs E_γ (GeV) photon beam energy. Superscripts are statistical errors and subscripts are systematic errors.

E_γ (GeV)	$\sqrt{s}$ (GeV)	$d\sigma/dt(\|t\| = \|t\|_{\min})$ (μb/GeV^2)	B (GeV^{-2})
1.6500	1.9942	$0.4015^{\pm 0.0170}_{\pm 0.0156}$	$3.1636^{\pm 0.3334}_{\pm 0.1249}$
1.7500	2.0407	$0.5605^{\pm 0.0280}_{\pm 0.0327}$	$3.1036^{\pm 0.3358}_{\pm 0.1742}$
1.8500	2.0861	$0.6796^{\pm 0.0206}_{\pm 0.0599}$	$2.8647^{\pm 0.1548}_{\pm 0.3436}$
1.9500	2.1306	$0.9525^{\pm 0.0219}_{\pm 0.0725}$	$3.8019^{\pm 0.0964}_{\pm 0.2544}$
2.0500	2.1742	$0.9088^{\pm 0.0353}_{\pm 0.1082}$	$3.5221^{\pm 0.1557}_{\pm 0.4297}$
2.1500	2.2170	$0.8779^{\pm 0.0229}_{\pm 0.0609}$	$3.1348^{\pm 0.0866}_{\pm 0.2139}$
2.2500	2.2589	$0.7138^{\pm 0.0300}_{\pm 0.0448}$	$2.8456^{\pm 0.1232}_{\pm 0.1924}$
2.3500	2.3001	$0.5735^{\pm 0.0304}_{\pm 0.0357}$	$2.2987^{\pm 0.1429}_{\pm 0.2173}$
2.4500	2.3405	$0.7866^{\pm 0.0230}_{\pm 0.0383}$	$2.2048^{\pm 0.0659}_{\pm 0.1144}$
2.5500	2.3803	$0.7069^{\pm 0.0559}_{\pm 0.0545}$	$2.6593^{\pm 0.1549}_{\pm 0.1585}$
2.6500	2.4193	$0.9782^{\pm 0.1859}_{\pm 0.0608}$	$3.0617^{\pm 0.3422}_{\pm 0.1524}$
2.7500	2.4578	$0.0389^{\pm 0.1518}_{\pm 0.0582}$	$3.1467^{\pm 0.2874}_{\pm 0.1416}$
2.8500	2.4957	$1.1070^{\pm 0.1065}_{\pm 0.0540}$	$3.4009^{\pm 0.2001}_{\pm 0.1412}$
2.9500	2.5330	$1.1376^{\pm 0.1309}_{\pm 0.0814}$	$3.2025^{\pm 0.2366}_{\pm 0.1498}$
3.0500	2.5698	$1.5404^{\pm 0.2722}_{\pm 0.1235}$	$3.8577^{\pm 0.3594}_{\pm 0.1835}$
3.1500	2.6061	$1.1367^{\pm 0.1662}_{\pm 0.1220}$	$3.1332^{\pm 0.2685}_{\pm 0.1820}$
3.2500	2.6418	$1.3291^{\pm 0.2542}_{\pm 0.1479}$	$3.1422^{\pm 0.3412}_{\pm 0.1903}$
3.3500	2.6771	$1.5029^{\pm 0.5328}_{\pm 0.2504}$	$3.2923^{\pm 0.5067}_{\pm 0.4077}$
3.4500	2.7119	$1.7548^{\pm 0.5939}_{\pm 0.2266}$	$3.3680^{\pm 0.4705}_{\pm 0.3440}$
3.5500	2.7463	$0.8867^{\pm 0.2394}_{\pm 0.2558}$	$2.8285^{\pm 0.3924}_{\pm 0.4753}$

[1] A. Klein, Phys. Rev. **99**, 998 (1955).
[2] G. Sterman *et al.*, Rev. Mod. Phys. **67**, 157 (1995).
[3] A. H. Mueller, Phys. Rep. **73**, 237 (1981).
[4] G. R. Farrar *et al.*, Nucl. Phys. B **349**, 655 (1991).
[5] B. Saghai, J.-C. David, B. Juliá-Diaz, and T.-S. H. Lee, Eur. Phys. J. A **31**, 512 (2007).
[6] J. Barth *et al.* (SAPHIR Collaboration), arXiv:nucl-th/9707025.
[7] T. C. Jude, J. Phys.: Conf. Ser. **349**, 012012 (2012).
[8] J. J. Xie, B. S. Zou, and H. C. Chiang, Phys. Rev. C **77**, 015206 (2008).
[9] C. S. An and B. S. Zou, Eur. Phys. J. A **39**, 195 (2009).
[10] Y. Oh, J. Korean Phys. Soc. **43**, S20 (2003).
[11] N. Isgur and G. Karl, Phys. Lett. B **72**, 109 (1977).
[12] S. Janssen, J. Ryckebusch, D. Debruyne, and T. Van Cauteren, Phys. Rev. C **65**, 015201 (2001).
[13] S. Capstick, Phys. Rev. D **46**, 2864 (1992).
[14] A. Kiswandhi and S. N. Yang, Phys. Rev. C **86**, 015203 (2012).
[15] N. Isgur and H. B. Thacker, Phys. Rev. D **64**, 094507 (2001).
[16] A. I. Titov and T.-S. H. Lee, Phys. Rev. C **67**, 065205 (2003).
[17] A. I. Titov, T. S. H. Lee, and H. Toki, Phys. Rev. C **59**, R2993 (1999).
[18] A. I. Titov, T. Nakano, S. Date, and Y. Ohashi, Phys. Rev. C **76**, 048202 (2007).
[19] R. A. Williams, Phys. Rev. C **57**, 223 (1998).
[20] J. Beringer *et al.*, Phys. Rev. D **86**, 010001 (2012).
[21] J. Barth *et al.* (SAPHIR Collaboration), Eur. Phys. J. A **17**, 269 (2003).
[22] T. Mibe *et al.* (LEPS Collaboration), Phys. Rev. Lett. **95**, 182001 (2005).
[23] D. P. Barber *et al.*, Z. Phys. C **12**, 1 (1982).
[24] J. Ballam *et al.*, Phys. Rev. D **7**, 3150 (1973).
[25] H. J. Besch *et al.*, Nucl Phys. B **70**, 257 (1974).
[26] H.-J. Behrend *et al.*, Nucl. Phys B **144**, 60 (1978).
[27] E. Anciant *et al.* (CLAS Collaboration), Phys. Rev. Lett. **85**, 4682 (2000).
[28] J. Breitweg *et al.* (ZEUS Collaboration), Eur. Phys. J. C **14**, 213 (2000).
[29] Hui-Young Ryu *et al.*, Prog. Theor. Exp. Phys. **2014**, 023D03 (2014).
[30] B. A. Mecking *et al.*, Nucl. Instrum. Methods Phys. Res., Sect. A **503**, 513 (2003).
[31] D. I. Sober *et al.*, Nucl. Instrum. Methods Phys. Res., Sect. A **440**, 263 (2000).

[32] Y. G. Sharabian *et al.*, Nucl. Instrum. Methods Phys. Res., Sect. A **556**, 246 (2006).
[33] E. Smith *et al.*, Nucl. Instrum. Methods Phys. Res., Sect. A **432**, 265 (1999).
[34] M. Amarian *et al.*, Nucl. Instrum. Methods Phys. Res., Sect. A **460**, 239 (2001).
[35] M. D. Mestayer *et al.*, Nucl. Instrum. Methods Phys. Res., Sect. A **449**, 81 (2000).
[36] D. S. Carman *et al.*, Nucl. Instrum. Methods Phys. Res., Sect. A **419**, 315 (1998).
[37] L. M. Qin *et al.*, Nucl. Instrum. Methods Phys. Res., Sect. A **367**, 316 (1995).
[38] F. J. Barbosa *et al.*, Nucl. Instrum. Methods Phys. Res., Sect. A **323**, 191 (1992).
[39] G. Adams *et al.*, Nucl. Instrum. Methods Phys. Res., Sect. A **465**, 414 (2001).
[40] R. De Vita *et al.* (CLAS Collaboration), Phys. Rev. D **74**, 032001 (2006).
[41] H. Seraydaryan, Ph.D. thesis, Old Dominion University, 2011.
[42] J. Ball and E. Pasyuk, CLAS Note No. 2005-002, 2005.
[43] R. De Vita and M. Battaglieri, CLAS Note No. 2009-105, 2009.
[44] M. Williams *et al.* (CLAS Collaboration), Phys. Rev. C **80**, 065208 (2009).
[45] M. Williams, Ph.D. thesis, Carnegie Mellon University, 2007.
[46] M. E. McCracken *et al.*, Phys. Rev. C **81**, 025201 (2010).
[47] M. Williams *et al.*, Phys. Rev. C **80**, 045213 (2009).